Soft Matter

Accepted Manuscript

ROYAL SOCIETY OF CHEMISTRY

www.rsc.org/softmatter

A graphical and textual abstract for the Table of contents entry

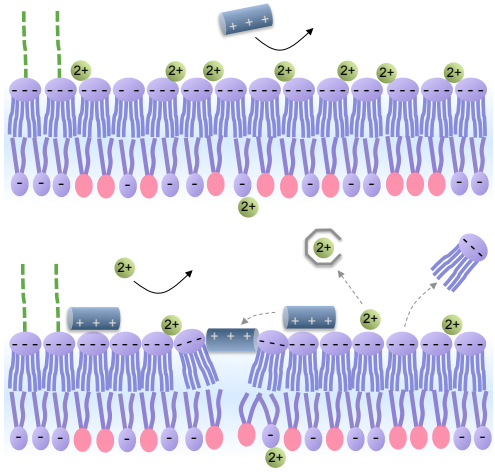

Fig. 8 Electrostatic modification of outer membrane permeability. At high concentrations, Mg^{2+} ions tighten and stabilize the outer LPS layer (upper panel). Under different conditions, cationic molecules (e.g., antimicrobial peptides) and EDTA can displace Mg^{2+} ions from the LPS layer, permeabilizing the outer membrane (lower panel).

ARTICLE TYPE
www. rsc.org/xxxxxx | XXXXXXXX

Electrostatic modification of the lipopolysaccharide layer: competing effects of divalent cations and polycationic or polyanionic molecules †

Norman Lam,[a†] Zheng Ma,[a‡] and Bae-Yeun Ha[a*]

Received Xth XXXXXXXXXX 20XX, Accepted Xth XXXXXXXXX 20XX
First published on the web Xth XXXXXXXXXX 200X
DOI: 10.1039/b000000x

The outer membrane (OM) of Gram-negative bacteria is asymmetrical with its outer layer mainly populated with polyanionic lipopolysaccharide (LPS). Much empirical evidence shows how OM permeability can be altered electrostatically: if Mg^{2+} or divalent cations are required for the integrity of the OM, antimicrobial peptides (AMPs) or ethylene-diaminetetraacetic acid (EDTA) can permeabilize it. Using a coarse-grained model of the outer LPS layer, in which the layer is viewed as forming discrete binding sites for opposite charges, we study how the LPS layer can be modified electrostatically. In particular, we capture systematically ion-pairing and lateral-charge correlations on the LPS layer. Our results offer a clear picture of (competitive) ion binding onto the LPS layer and its impact on the lateral packing of LPS molecules, similarly to what has been seen in experiments: divalent cations such as Mg^{2+} not only neutralize the LPS layer but also make its planar charge distribution heterogeneous, thus tightening the LPS layer; on the other hand, polycationic AMPs or polyanionic EDTA can displace Mg^{2+} ions from the LPS layer and counteract the favorable effect of Mg^{2+}. Our result will be useful for clarifying to what extent OM permeability can be modified electrostatically.

1 Introduction

The outer membrane (OM), enclosing Gram-negative bacteria, is highly asymmetrical: while phospholipids are localized to the inner layer, lipopolysaccharide (LPS) is the main component of the outer layer[1–5]. The resulting OM is nominally resistant to harmful foreign molecules such as antibiotics and lysozyme. The permeability is, however, determined not only by its intrinsic properties but also by its interaction with ions and ionic molecules such as Mg^{2+}, ethylenediaminetetraacetic acid (EDTA) *, antibiotics, and antimicrobial peptides (AMPs)[3–13]. The polyanionic nature of LPS is intriguingly implicated – the resulting cation-binding ability of LPS has both favorable and adverse effects. If Mg^{2+} (or Ca^{2+}) is essential for the integrity of the LPS layer and the OM, the presence of EDTA or cationic AMPs can diminish the integrity[3–13]; these LPS-perturbing agents, especially EDTA, can lead to release of LPS in the medium[3,4,8,9] (see Fig. 1).

Electrostatic modification of LPS stability is relevant in a various contexts: (i) susceptibility and resistance of Gram-negative bacteria to antimicrobial agents[3–15] and (ii) their adaptation to an Mg^{2+}-limiting environment[15,17]. Lipid-charge neutralization is often a common theme for developing bacterial resistance, by which the binding of antimicrobials to lipid charges is disrupted[18], affecting (i), and for diminishing the adverse electrostatic effect arising from lipid-charge repulsions in both (i) and (ii).

While the precise mechanism of their action is not known yet, amphiphilic AMPs or peptide antibiotics are believed to permeabilize the OM of Gram-negative bacteria in the following three distinct steps: (i) electrostatic binding onto the LPS layer leading to Mg^{2+} displacement[3,4,12], (ii) hydrophobic insertion into the LPS layer, partially facilitated by the first step, and structural changes of the LPS layer[3–5,8], and (iii) permeabilization of the OM via pore formation or perturbation of a bilayer structure, possibly allowing lipid exchanges between the OM and the inner one[8,15,16] (see Fig. 1 as well as Fig. 7 in Ref.[15] and Fig. 2 in Ref.[8]).

Despite its significance, however, beyond the empirical evidence[19–22] (also see Refs.[3–13]), the physical effects arising from ions and polyions on LPS have not been well understood, especially in a quantitative manner. Ion (K^+ or Mg^{2+}) distributions near LPS layers have been the main focus of a few earlier studies[23,24] but their impact on the LPS layer has remained to be explored.

Here, we present a systematic theoretical approach to elec-

† Electronic Supplementary Information (ESI) available: [details of any supplementary information available should be included here]. See DOI: 10.1039/b000000x/

[a] *Department of Physics and Astronomy, University of Waterloo, Waterloo, Ontario N2L 3G1, Canada.*
[†] *Department of Physics, University of Toronto, Toronto, Ontario M5S 1W4, Canada.*
[‡] *Current address: Department of Physics, University of Ottawa, Ontario K1N 6N5, Canada.*
[*] *Corresponding author; Email: byha@uwaterloo.ca.*

* It typically carries four negative charges in solution and can be found in the form $EDTA^{4-}$.

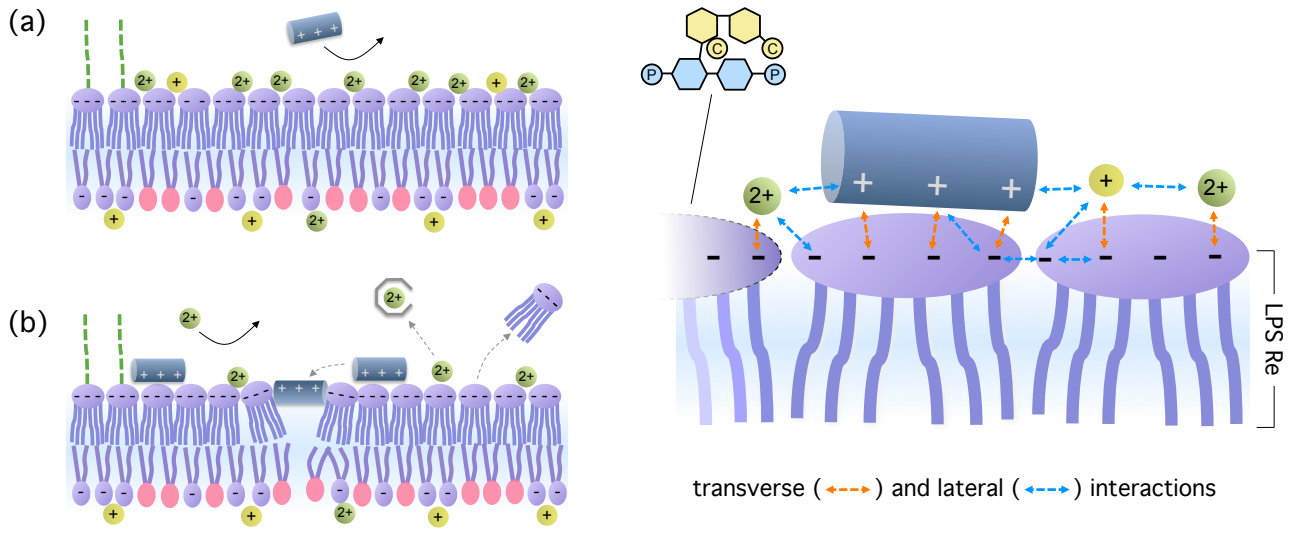

Fig. 1 The outer membrane of Gram-negative bacteria and competing effects of Mg^{2+} and AMPs on the membrane. Refer to Fig. 2(a) in this work and Fig. 1 in Ref. [1] for more molecular details of LPS; here each oval shape contains all (four) charges on lipid A and in the 'inner core.' (a) At high Mg^{2+} population on the surface, AMP binding is hindered and the Mg^{2+}-stabilized LPS layer serves as a "protective coat" against AMPs and other polycations. (b) At high concentrations, AMPs, polycations, or EDTA (open polygon in grey) can displace competitively divalent ions from the LPS surface. As a result, the tightening effect of the divalent ions is reduced and membrane integrity compromised, easing AMP's penetration through the membrane. On the right, transverse and lateral interactions are represented by dashed arrows. While the peptide shown is polyvalent, each cationic residue is naturally assumed to be paired with one backbone charge. On the illustration the top, the headgroup of LPS Re is shown, where P refers to phosphate groups and C carboxyl groups (see also Fig. 2).

trostatic modification of the LPS layer: the competitive electrostatic binding among Na^+, Mg^{2+}, and cationic AMPs or polycations; Mg^{2+} depletion by EDTA; their effects on the lateral packing of LPS. This electrostatic aspect, which underlines the first step (i) in membrane permeabilization, merits much consideration, because of its impact on the next steps it follows. To put this in a broader context, it is worth recalling related phenomena. For instance, divalent cations diminish water penetration through LPS layers or decrease LPS chain mobility [20,21]. Also, the aggregation state of LPS molecules can be tuned through electrostatic effects, possibly in a salt-dependent way [2,3,22,25,26]. Similarly, lipid-tail ordering can be induced by Mg^{2+}, which is manifested by an increase in the melting temperature from the gellike to liquid crystalline phases [2,3].

Accordingly, our main focus here is placed on examining to what extent the LPS layer can be modified *electrostatically*. Along this line, it is worth clarifying the scope of this work. In the absence of AMPs, our effort will offer a systematic (free-energy) approach to the LPS system, which takes into account a few important details such as finite ionic sizes as well as transverse and lateral interactions (see Fig. 1). In the presence of AMPs or other amphiphilic molecules, such an effort will be beneficial for clarifying how much of LPS or OM perturbations can be attributed to their electrostatic interaction with the LPS layer. This will be particularly useful for understanding the competing effects of Mg^{2+} and polycations on OM permeability despite their common cationicity [3–13]. Note that our understanding of such a complex system does not go much beyond the simpler problem of simple-ion binding onto an oppositely-charged surface [27,28]. We thus leave for future work other complications such as the hydrophobic insertion of AMPs into the LPS layer and its impact on the OM as a whole (see Fig. 1(b)). † Nevertheless, our work will form a first step toward modelling more realistically OM permeability, since the electrostatic effects we focus on will remain relevant, largely independently of other complexities. ‡ A re-

† Also we consider an already-formed LPS layer as a reference state. Clarifying the phase behaviour of LPS molecules in an aqueous solution is outside the scope of our work [2,3,22,25,26], even though it would reflect similar electrostatic effects.

‡ To improve on our approach, a more complete (theoretical) understanding of the energetics that underlies asymmetric-OM perturbations, especially by amphiphilic molecules (e.g., AMPs), will be required (see Refs. [5,16,31] for experimental efforts). In particular, this would necessitate a theoretical model for describing the hydrophobic incorporation of AMPs into the OM at the level comparable to the one often used for the better-known problem: AMP interactions with and insertion into a (symmetric) phospholipid membrane in a fluid state (see Refs. [30,32,33] and references therein). Indeed, the electrostatic and hydrophobic adsorption of cationic APMs into such a (symmetric) membrane has only recently been formulated [33].

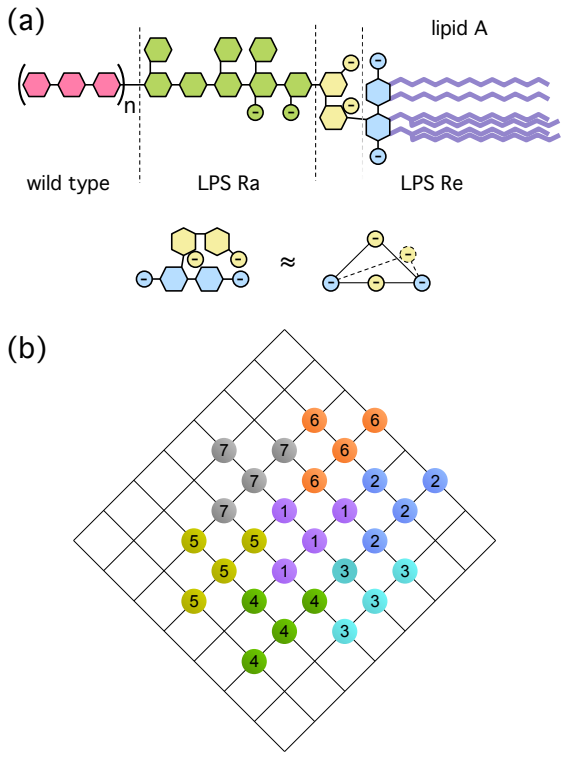

Fig. 2 Modelling the LPS layer as binding sites for opposite charges: (a) molecular structure of LPS and its charges, and (b) "decoration" of a lattice with LPS charges. Each hexagon represents a sugar molecule: glucosamine in light blue, Kdo in yellow, ... The top panel in (a) is adapted with modifications from Ref.[25]. (See Refs.[1–3] for more details.) For simplicity, we limit ourselves to LPS Re as shown in (a) and invoke the following simplification: we treat the four charged groups on LPS to lie approximately on the vertices of an isosceles right triangle, as depicted in the bottom panel in (a), and tilt the triangle so as to fit into the square lattice as shown in (b), where the numbers 1, 2, 3, ... are to keep track of charges belonging to the same LPS molecule.

lated point is that to some extent the permeability property of a bilayer is regulated independently by the two individual layers[29]. As a result, one may gain useful insight into OM permeability by studying (symmetric) LPS bilayers[16,19,20] or focusing on the outer LPS layer.

Much effort is made here to capture systematically the (long-ranged) electrostatic interactions between bound charges on the LPS surface such as AMP-AMP repulsions and Mg^{2+}-AMP repulsions in a wide parameter space. In our course-grained picture, LPS charges are viewed as forming a two-dimensional (square) lattice, as illustrated in Fig. 2, attracting opposite charges. Following up on Refs.[27,28], we capture such important details as charge discreteness, ionic sizes, and ion pairing on the LPS layer (e.g., between an LPS charge and Mg^{2+}); importantly, we develop a new scheme for taking into account the lateral correlations between Mg^{2+}-paired and Mg^{2+}-free LPS charges. The resulting approach requires non-trivial generalizations of existing theoretical approaches to ion binding to an oppositely-charged surface[27,28], as evidenced below.

Using this coarse-grained model, we calculate the surface coverage of these ions or ionic molecules as well as the electrostatic contribution to the lateral pressure $\Delta\Pi$, as a function of their bulk concentrations. The physical picture emerging from our free energy approach is as follows. In the presence of monovalent ions only, $\Delta\Pi > 0$ over a wide or practically-entire range of ion concentrations, meaning that the lipid headgroups are swollen by the electrostatic repulsion between LPS charges. The binding of Mg^{2+} onto a charge on LPS inverts the sign of the charge (see Fig. 1 on the right). This makes the LPS surface charge heterogeneous, which turns the repulsion between adjacent LPS charges into an attraction ($\Delta\Pi < 0$), tightening the LPS layer.

Our results for $\Delta\Pi$ are consistent with and thus offer a quantitative basis of several observations mentioned earlier (e.g., diminished water penetration through LPS layers or decreased LPS chain mobility, in the presence of divalent cations)[20–22,25]. Importantly, it is well aligned with the long-standing observation that the presence of divalent cations increases bacterial resistance against cationic AMPs or other membrane-perturbing agents[3–13].

On the other hand, we find that cationic AMPs of large valence or EDTA can displace Mg^{2+} from the LPS layer competitively or by chelation[3,4,12] and counterbalance the favorable effect of Mg^{2+}, resulting in $\Delta\Pi > 0$, more so at high concentrations of these molecules in bulk. This is consistent with the general picture of these molecules as LPS perturbing agents[3–13]. Furthermore, this finding may shed a quantitative insight into the release of LPS into the medium by EDTA long observed in the literature[3,4,8,9]. When $\Delta\Pi > 0$, individual LPS headgroups are swollen by the repulsion between their negative changes. This creates an optimal-area mismatch be-

tween the inner and outer layers, leading to LPS release (see Refs.[3,4,8] for other LPS-releasing agents). Finally, our finding of $\Delta\Pi > 0$ in the presence of AMPs may offer a quantitative basis of how they can gain entry into the cytoplasmic membrane to exert their antimicrobial activity[12,13,34].

This paper is organized as follows. In Sec. 2, we present a coarse-grained model of the LPS layer interacting with the surrounding ions and molecules. Our results for the competitive binding and its effects on LPS are presented in Sec. 3.

2 Modelling the LPS layer

2.1 LPS as binding sites

LPS molecules are amphiphilic, each typically consisting of lipid A (or endotoxin), a short 'core' oligosaccharide, and a possibly-long distal polysaccharide[1–3], as illustrated in Fig. 2(a). In this figure, colored hexagons are used to represent different sugar molecules; in Fig. 1, they are shown for a few LPS molecules (dashed green lines). Lipid A, the 'hydrophobic anchor' of LPS[1], is formed by several (typically 4-6 or 7) hydrocarbon chains on one end and two anionic phosphorylated GluN (glucosamine) units on the other. In LPS Re (deep rough mutant lipopolysaccharide), two additional anionic Kdo (2-keto-3-deoxyoctonoic) units are covalently-bonded with one of GluN units, forming the 'inner core.' LPS Ra (rough mutant lipopolysaccharide) contains additional eight saccharide units in the 'outer core' with two of them phosphorylated. Only wild-type LPSs carry polydisperse O-saccharide chains at the outmost domain. (See Refs.[1–3,22] for more details and other LPS types.)

LPS Re is the simplest form of LPS required for bacterial growth[1]. Thus, we mainly focus on LPS Re, each carrying four ionizable groups, as illustrated in Fig. 2(a): two phosphate groups (in light blue) and two carboxyl groups (in yellow). This will not, however, limit severely the applicability of our work, since the electrostatic effects on LPS we focus on are not sensitive to other details (also see below).

Here, we invoke the following simplification: the four charged groups on LPS are taken to lie approximately on the vertices of an isosceles right triangle, as depicted in the middle panel in Fig. 2. Such triangles are tilted onto a square lattice as shown in Fig. 2(b), where the numbers 1, 2, 3, ... are to keep track of charges belonging to the same LPS molecule. [In fact, the plane of carboxyl groups (yellow balls) is a few angstrom away from that of phosphate groups (light blue balls). But this is ignored in our model.] A more accurate charge arrangement, referred to as 'minimum model,' was used (Ref.[24] and references therein). If this model is more suitable for numerical studies, the square-lattice model is analytically tractable. An accurate description of ion distributions would necessitate a more accurate model. However, our main focus is on examining how various competing effects influence the LPS layer. Along this line, it is worth mentioning that unlike specific (chirality-dependent) interactions, the electrostatic interaction is more generic and will not sensitively depend on how backbone charges are arranged (i.e., square vs. hexagonal lattices). For this reason, the outcome of our approach will remain relevant to other LPS systems. Moreover, as evidenced later, other details such as ionic sizes or charge discreteness are (more) crucial to capture (see also Refs.[27,28,35]).

As for its electrostatic properties, we view the LPS layer as *discrete* electrostatic binding sites on a square lattice for opposite charges, so as to capture both lateral and transverse interactions among surface charges, i.e., both lipid charges and cationic charges without suppressing important details. (See the panel on the right in Fig. 1 for the meaning of transverse and lateral interactions). Indeed, a number of theoretical studies highlight the significance of charge discreteness, especially in the presence of multivalent ions[27,28,35]. This detail not only enhances ion binding[27,28] but also creates charge heterogeneity on the surface[35]. It was even shown that charge heterogeneity is responsible for Mg^{2+}-stabilized reverse hexagonal (H_{II}) phases of phosphatidylserine (PS), which would otherwise form lamellar phases[35]. Furthermore, it was even suggested that the ion specificity between Mg^{2+} and Ca^{2+} can be explained via ion sizes[28]. Even though the former is smaller in size by itself, it has a larger (effective) hydrated radius. As a result, Ca^{2+} binds more strongly to an anionic charge.

We first introduce a simple (Langmuir-type) binding model[36,37], ignoring the long-range nature of Coulomb forces. The resulting model is equivalent to keeping transverse interactions only, while omitting lateral interactions. Consider two types of ions, which are oppositely charged: A and B. Let AB denote an ion pair and K the association or ion-binding constant (see Fig. 3(a)). Let us assume that free ions are "ideal gases" and ion pairing is solely governed by Coulomb forces[28,38].

It proves useful to introduce the Bjerrum length (see for instance Ref.[36]) defined as

$$\ell_B = \frac{e^2}{4\pi\varepsilon_0\varepsilon_r k_B T}, \tag{1}$$

where ε_0 is the permittivity of free space, ε_r is the dielectric constant of a solvent, and k_BT is the thermal energy. A standard choice for K is

$$K = 4\pi \int_d^{|Z_A Z_B|\ell_B/2} dr r^2 \exp\left(\frac{|Z_A Z_B|\,\ell_B}{r}\right), \tag{2}$$

where Z_A and Z_B are the valences of A and B, respectively[28,38]. Note that we introduced $r_{\min} = d$ as the minimum distance between the two charges in an ion pair, so as to avoid a singularity at $r = 0$, which is unphysical. On the other

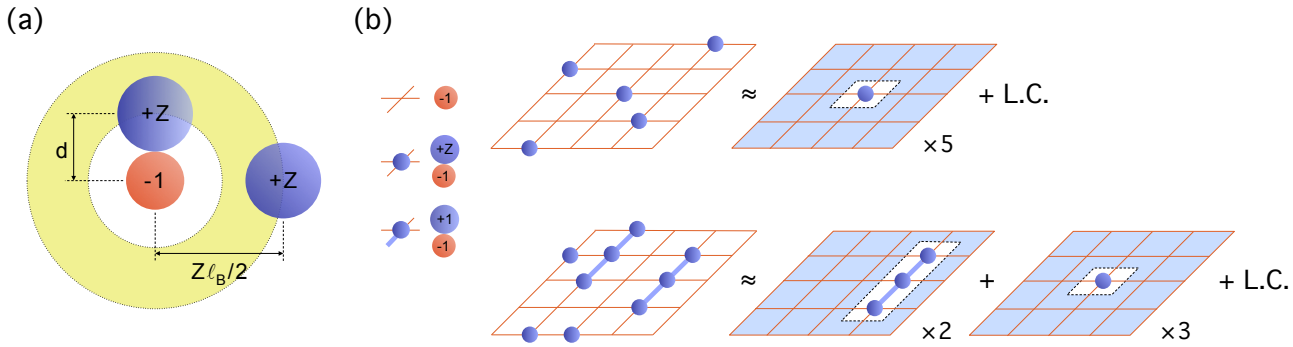

Fig. 3 Ion pairing in free space (a) and ion pairing/binding on the LPS layer (b). (a) A conventional view of ion pairing is illustrated. The yellow ring represents the ion-pairing region: if the center of the cation in blue is within the yellow ring, the ion is considered electrically bound or paired, since its attractive interaction is larger in magnitude than k_BT; if the center is outside, it is then free. A plausible simplification amounts to assuming that the ion pair is kept at a fixed distance δ. By appropriately choosing δ, this picture can map onto the original one in (a). (b) The ion-pairing idea in (a) can be extended to ion pairing/binding on a (discretely) charged surface, e.g., the LPS layer. In the lower panel, a bound peptide is represented as a linear connection of a few charges. Besides the transverse interaction between ion pairs, however, the lateral interaction with other surrounding (backbone or bound) charges also influences ion binding on the surface, as illustrated in Fig. 1 on the right. The lateral interaction at the meanfield level or in the continuum limit is illustrated by the lattice with a light blue background. In this picture, the lateral interaction within each site or in the small white region should be omitted, since this interaction is either included in the transverse interaction term through an ion-pairing term or a self-energy term in the discrete limit. Finally, the lateral interaction beyond the meanfield approximation or a lateral correlation (L.C.) term will have to be included (see Fig. 4 for our scheme for calculating this term).

hand, the upper limit $r_{\max} = |Z_A Z_B|\,\ell_B/2$ was chosen to coincide with the distance at which the Coulomb energy becomes K_BT. Within this distance, the two charges are considered as "bound."

Once K is known, the concentration of AB or ion pairs can be determined by

$$K = \frac{[\mathrm{AB}]}{[\mathrm{A}]\,[\mathrm{B}]}, \tag{3}$$

where $[...]$ denotes the concentration of species .... If $N_{...}$ is the number of species ... in a volume V, $[\mathrm{A}] = N_A/V$, $[\mathrm{B}] = N_B/V$, and $[\mathrm{AB}] = N_{AB}/V$. This can be rewritten as

$$\ln([\mathrm{A}]\,v) + \ln([\mathrm{B}]\,v) = \ln([\mathrm{AB}]\,v) - \ln\left(\frac{K}{v}\right), \tag{4}$$

where v, a typical volume for ions, is needed to make each term dimensionally correct. This equation simply means chemical equilibrium between the two ion species: "free" and "paired."

Note that $-k_BT\ln(K/v)$ is the free energy of an ion pair. In a simplified picture, the paired ions are kept at a fixed distance δ from each other[27,28]. By appropriately choosing δ, these two picture can map onto each other. So there is no essential difference between the two pictures.

Now assume that ions of type B are fixed in space and arranged on a lattice (e.g., LPS charges); if B represents unoccupied charges, AB denotes occupied sites. If N_0 is the total number of binding sites whether occupied or not, then $N_0 = N_{AB} + N_B \equiv N + (N_0 - N)$. First, assume that A interacts with one of B's. Then Eq. 4 can be used for this case:

$$\ln([\mathrm{A}]\,v) = \ln\left(\frac{\theta}{1-\theta}\right) - \ln\left(\frac{K}{v}\right), \tag{5}$$

where $\theta = N/N_0$ is the fraction of occupied sites. If only transverse interactions are included, θ can readily be obtained, once K in Eq. (2) is calculated.

2.2 Lateral vs. transverse interactions

Because of the long-range nature of electrostatic interactions, Eq. 5 remains relevant in a high-salt limit, where Coulomb interactions are sufficiently screened. In principle, it is straightforward to list all pair interactions between charges on the surface, both backbone charges as well as bound charges. The electrostatic energy of a charge distribution is given as a pairwise sum of these interactions (screened by the surrounding salt ions). The electrostatic free energy F_{elec} can then be expressed as a sum over all charge arrangements weighed with the Boltzmann factor[39]. The resulting free energy F_{elec} is to be minimized with respect to a few parameters: N_1 (the number of bound Na^+ ions), N_2 (the number of bound Mg^{2+} ions), and N_p (the number of bound peptides).

In the past, several theoretically tractable models have been proposed for studying ion binding (see Refs. [27,28] and those therein). Unfortunately, none of them is well suited for the

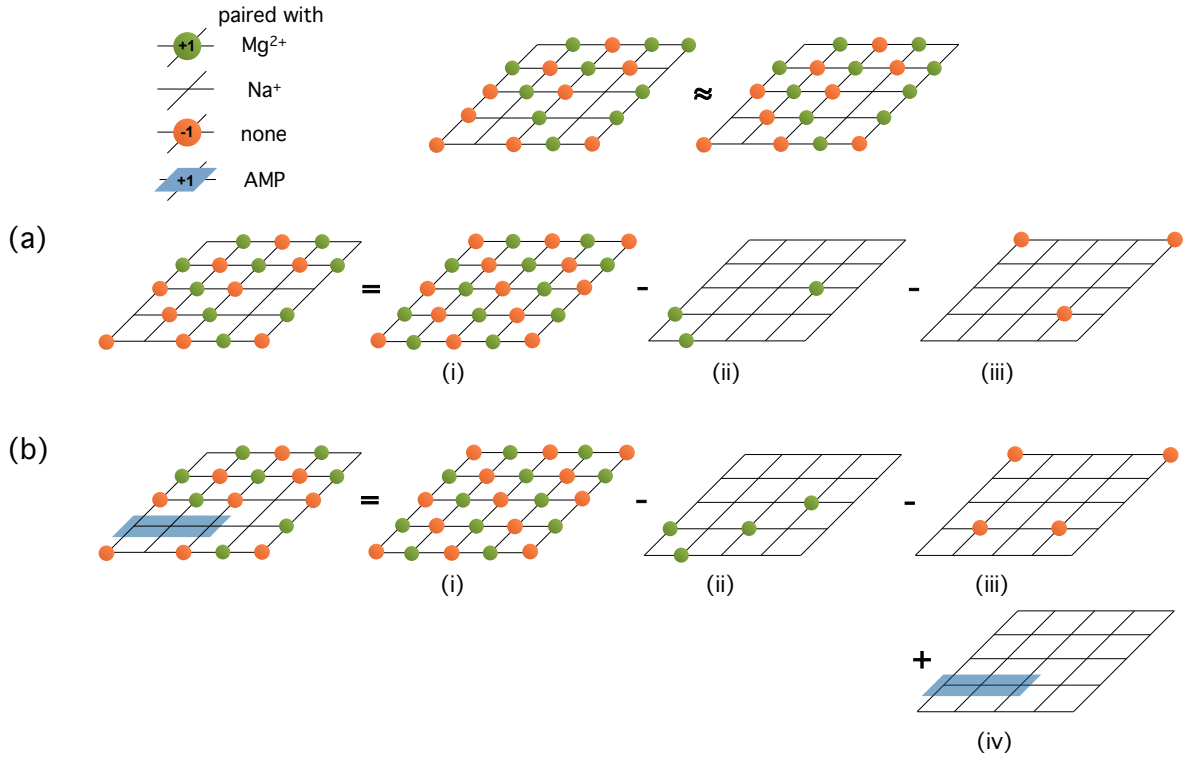

Fig. 4 Theoretical scheme for counting the lateral interaction energy of the LPS layer in the presence of Mg^{2+} and in the absence (a) or presence (b) of AMPs. Mg^{2+}-paired backbone charges are shown in green and unpaired backbone charges in tangerine; empty sites are occupied by Na^{+} and shaded sites by AMPs, both carrying zero net charge. Mg^{2+} pairing at a given site inverts the sign of charge there from -1 to $+1$. The total electrostatic energy of a given charge arrangement is a pairwise sum of screened Coulomb interactions over all sites (green, tangerine, empty, and shaded) on the lattice; the free energy is then given as a sum over all charge arrangements weighed with the Boltzmann factor. Here we invoke a physics-inspired simplification, as illustrated on the top: we rearrange a charge distribution (left) close to a "perfect" one (right), where the sign of charge alternates regularly on the lattice except on neutral sites. The resulting charge configuration is an energy-minimizing one and can be expressed as a superposition of two parts: a perfect neutral lattice with equal numbers of green and red sites (i) and a lattice with one kind of charge (ii) & (iii).

LPS system. Here, we present a new scheme, which requires non-trivial generalizations of the existing ones[27,28]. To this end, we first decompose $F_{\rm elec}$ into meanfield ($F_{\rm MF}$), transverse ($F_{\rm trans}$), and lateral-correlation terms ($F_{\rm LC}$).

While the detailed derivation is presented in the Appendix, here we capture the essence of our theoretical scheme for calculating $F_{\rm elec}$. A meanfield approximation, which amounts to smearing out the surface charges, fails to capture an important feature of this system: charge discreteness, especially for Mg^{2+}-backbone charge pairs, also referred to as transverse interaction. This effect not only enhances Mg^{2+} binding at a given site but also inverts the sign of change at the site. It thus gives rise to charge inhomogeneity on the surface, i.e., an overall-cationic Mg^{2+}-anionic lipid pair surrounded by possibly unpaired anionic LPS charges. This induces an attraction between neighbouring LPS molecules, which would otherwise repel each other. This lateral-correlation effect is responsible for Mg^{2+}-stabilization of the LPS layer, a salient feature of Mg^{2+} binding.

In our approach, $F_{\rm elec}$ is given as a linear superposition of $F_{\rm MF}$, $F_{\rm trans}$, and $F_{\rm LC}$: $F_{\rm elec} = F_{\rm MF} + F_{\rm trans} + F_{\rm LC}$. First note that the ion-pairing idea in Fig. 3(a) can be applied to ion pairing or transverse interactions on a (discretely) charged surface such as the LPS layer, as illustrated in Fig. 1 (see the panel on the right). The main difference is that paired ions on the surface have less degrees of freedom compared to those in bulk[28]. Besides the transverse interaction, the lateral interaction with other surrounding (backbone or bound) charges also influences ion binding on the surface (see the panel on the right in Fig. 1). The lateral interaction at the meanfield level or in the continuum limit is illustrated in Fig. 3(b) (see the lattice with a light blue background). Crudely speaking, we smear out all surface charges and calculate the electrostatic energy stored[27] – to avoid double counting in this approach, the lateral interaction within each site or in the small white region should be omitted. This interaction is included either in the transverse interaction (ion-pairing term) of pair sites or a self-energy term of unpaired sites in the discrete limit. This consideration enables one to calculate $F_{\rm MF}$ and $F_{\rm trans}$.

In our view, the charge-neutralizing effect of AMPs in Fig. 3(b) (lower panel) is similar to that of a series connection of a few Na^+'s, since individual charges on AMPs are monovalent. Thus in our approach, there is no qualitative difference between AMPs and Na^+.

A method for calculating the lateral interaction beyond the meanfield level or simply the lateral correlation term $F_{\rm LC}$ is outlined in Fig. 4, where the LPS layer is shown in the presence of Mg^{2+} and in the absence (a) or presence (b) of AMPs; see the Appendix for details. A few colors are used for different charge pairs: Mg^{2+}-bound sites are shown in green and unpaired backbone charges in tangerine; empty (electrically neutral) sites are those occupied by Na^+ and shaded sites by AMPs, both carrying zero net charge.

Based on physics grounds, we invoke simplifications: as illustrated on the top, we rearrange a charge distribution (left) close to an alternating one (right), where the sign of charge alternates regularly on the lattice, except on neutral sites. The resulting charge configuration is one that minimizes energy. Note that this lattice does not have to be overall neutral. As a result, the (free) energy of this lattice may not be solely determined by lateral correlations. (Recall $F_{\rm elec} = F_{\rm MF} + F_{\rm trans} + F_{\rm LC}$; unless the lattice is overall neutral, $F_{\rm MF}$ also contributes.) To focus on $F_{\rm LC}$, we decompose the lattice into two parts as illustrated in Fig. 4: a "perfect" neutral lattice with equal numbers of green and red sites arranged alternatively (i) and a lattice with one kind of charge (ii) & (iii). We then consider the perfect lattice (i) as a reference. Since this does not always represent the original one (on the left in Fig. 4 (a) or (b)) correctly, we need to make "corrections." The Appendix (subsection C. "Lateral correlations") shows how the corrections can be obtained systematically.

Based on the physical pictures in Figs. 3 and 4, we have derived $F_{\rm MF}$, $F_{\rm trans}$, and $F_{\rm LC}$, and presented the intermediate steps in the Appendix. Here and in what follows, these are free energies per site given in units of k_BT. In summary, they are given by

$$\begin{aligned} F_{\rm MF}\cdot\frac{N_0^2a^2}{\Delta\ell_B} &= \left(\frac{\pi}{\kappa}-\frac{\mathscr{M}_1}{2}\right)(N_0-N_1-2N_2-QN_p)^2-\frac{\mathscr{M}_p-\mathscr{M}_1}{2}QN_p(N_1+2N_2+QN_p)\\ F_{\rm trans}\cdot\frac{N_0}{\Delta\ell_B} &= -\frac{N_1}{\delta_1}-\frac{2N_2}{\delta_2}-\frac{QN_p}{\delta_p}\\ F_{\rm LC}\cdot\frac{N_0}{\Delta\ell_B} &= -2\frac{N_2(N_0-N_1-N_2-QN_p)}{N_0}\zeta(a). \end{aligned} \tag{6}$$

Here, various symbols are defined as follows. First, $\mathscr{M}_\nu$ ($\nu = 1$ or Q) is given by

$$\mathscr{M}_\nu(\kappa,a) = \int_{-a\nu/2}^{a\nu/2}dx\int_{-a/2}^{a/2}dy\frac{e^{-\kappa\sqrt{x^2+y^2}}}{\sqrt{x^2+y^2}}. \tag{7}$$

The terms containing $\mathscr{M}_v$ are to correct the electrostatic free energy for the over-counting of Coulomb interactions as noted earlier. Also, $\zeta(a)$ is an infinite sum given by

$$\zeta(a) = \frac{1}{2}\sum_{i=1}^{\infty}\sum_{j=0}^{i}(-1)^{i+j-1}\frac{e^{-\kappa a\sqrt{i^2+j^2}}}{a\sqrt{i^2+j^2}}\cdot k(i,j) \tag{8}$$

where $k(i,j)$ is defined as

$$k(i,j) = \begin{cases} 4 & \text{if } j=0 \text{ or } i=j \\ 8 & \text{otherwise} \end{cases} \tag{9}$$

Finally, Δ accounts for the effect of dielectric discontinuity. At the meanfield level, $\Delta = \frac{2(\eta+\kappa d)}{2\eta+\kappa d}$, where $\eta = \varepsilon_l/\varepsilon_w$ with ε_l and ε_w the dielectric constant of lipids and water, respectively; beyond the meanfield level, this can be understood as an interpolation and is accurate at the two limiting cases: $\eta = 1$ and $\eta = 0$. For practical purposes, it can be approximated as $\Delta \approx 2$, since $\eta \approx 0$ for the membrane-water system we consider. (An earlier study indicates that the effect of dielectric discontinuities depends on how they are treated[41]. For $\eta \ll 1$, however, $\Delta \approx 2$, largely independent of details.)

On the other hand, the entropic free energy of bound ions per site (in units of k_BT) is given by

$$\begin{aligned} F_{\text{ent}}\cdot N_0 &= N_1\ln\left(\frac{N_1}{N_0}\right)+N_2\ln\left(\frac{N_2}{N_0}\right)+N_p\ln\left(\frac{N_p}{N_0}\right)+(N_0-N_1-N_2-QN_p)\ln\left(1-\frac{N_1+N_2+QN_p}{N_0}\right) \\ &\quad +\frac{1-Q}{Q}(N_0-QN_p)\ln\left(1-\frac{QN_p}{N_0}\right). \end{aligned} \tag{10}$$

Note that the first two lines of Eq. 10 can be derived by considering the number of ways in which N_1 monovalent ions, N_2 divalent ions, and N_p peptides are arranged on a lattice with N_0 binding sites.

The chemical potentials of ions and peptides bound to the surface can readily be obtained as $\mu_i^s = \partial\left(F_{\text{elec}}+F_{\text{ent}}\right)/\partial\left(N_i/N_0\right)$ (in units of k_BT):

$$\begin{aligned} \mu_1^s &= \frac{\Delta\ell_B}{N_0a^4}\left[\left(\frac{2\pi}{\kappa}-\mathscr{M}_1\right)(-N_0+N_1+2N_2+QN_p)-\frac{(\mathscr{M}_p-\mathscr{M}_1)}{2}QNp\right] \\ &\quad -\frac{\ell_B\Delta}{\delta_1}+2\frac{\Delta\ell_B}{a^2}\left(\frac{N_2}{N_0}\right)\zeta(a)+\ln\frac{N_1}{N_0-N_1-N_2-QN_p}, \end{aligned} \tag{11}$$

$$\begin{aligned} \mu_2^s &= 2\frac{\Delta\ell_B}{N_0a^4}\left[\left(\frac{2\pi}{\kappa}-\mathscr{M}_1\right)(-N_0+N_1+2N_2+QN_p)-\frac{(\mathscr{M}_p-\mathscr{M}_1)}{2}QNp\right] \\ &\quad -\frac{2\ell_B\Delta}{\delta_2}+2\frac{\Delta\ell_B}{a^2}\left(\frac{N_1+2N_2+QN_p-N_0}{N_0}\right)\zeta(a)+\ln\frac{N_2}{N_0-N_1-N_2-QN_p}, \end{aligned} \tag{12}$$

$$\begin{aligned} \mu_p^s &= Q\frac{\Delta\ell_B}{N_0a^4}\left[\left(\frac{2\pi}{\kappa}-\mathscr{M}_1\right)(-N_0+N_1+2N_2+QN_p)-\frac{(\mathscr{M}_p-\mathscr{M}_1)}{2}(N_1+2N_2+2QN_p)\right] \\ &\quad -\Delta\ell_B\frac{Q}{\delta_p}+2Q\frac{\Delta\ell_B}{a^2}\left(\frac{N_2}{N_0}\right)\zeta(a)+\ln\frac{N_p\cdot(N_0-QN_p)^{Q-1}}{(N_0-QN_p-N_1-N_2)^Q}. \end{aligned} \tag{13}$$

As $\kappa\to\infty$, the last two terms in Eqs. 11 will remain relevant, as in Eq. 5.

On the other hand, the chemical potentials of free ions and peptides (in bulk) are given by

$$\mu_i^b(n_i) = \ln\left(C\cdot n_i\cdot\frac{4}{3}\pi r_i^3\right)-\frac{Z_i^2}{2}\frac{l_B}{\delta_i}(\Delta-1)-\frac{Z_i^2}{2}\frac{l_B\kappa}{1+\kappa r_i}, \tag{14}$$

$$\mu_p^b(n_p) = \ln(C\cdot n_pv_p)-\frac{Q}{2}l_B(\Delta-1)\left(\frac{1}{\delta_p}+\frac{\mathscr{M}_p-\mathscr{M}_1}{a^2}\right)-\frac{Q}{2}\frac{l_B\kappa}{1+\kappa r_1}, \tag{15}$$

where $C = 0.6022\,\text{nm}^{-3}\cdot\text{L/mol}$ is the conversion factor from molar concentration to number per volume, v_p is the volume of a peptide molecule, and r_i is the hydration radius of monovalent or divalent ions in bulk, respectively. Note that the second last

term on the right hand side of Eqs. 14 and 15 is the self-energy of free ions or peptides in bulk with reference to those on the LPS layer; the last term is the 'polarization' energy, the electrostatic free energy gain of a charged particle due to the shielding of its charge by the surrounding ions[36,37]. To some extent, $F_{\rm LC}$ can be viewed as a surface analogue of this term, except that $F_{\rm LC}$ is given in the discrete limit, since their origins are similar.

In equilibrium, $\mu_i^s = \mu_i^b$ and $\mu_p^s = \mu_p^b$. These relations can be solved simultaneously for N_i and N_p. In our analysis, we have chosen the parameters as follows: $\delta_1 = 3\,$Å, $\delta_2 = 2.5\,$Å, $r_1 = 3.4\,$Å, $r_2 = 4.3\,$Å[40] §, $Q = 4$ (as for magainin 2[12]), $v_p = 2.5\,{\rm nm}^3$.

3 Results and Discussion

How the LPS layer is electrostatically modified especially by Mg^{2+} and polycations can be quantified in terms of the excess lateral pressure (or tension) $\Delta\Pi$ arising from electrostatic interactions (both lateral and transverse) on the LPS layer. Let us now consider $F_{\rm elec}$ as the total electrostatic free energy of the LPS layer per binding site, already minimized with respect to N_i and N_p. Then $\Delta\Pi = -\partial F_{\rm elec}/\partial a$. If $\Delta\Pi > 0$, then the electrostatic effect is unfavorable to the LPS layer, while if $\Delta\Pi < 0$ it tightens the LPS layer.

In this work, we obtained $\Delta\Pi$ numerically based on the theory presented in Sec. 2. Let a_0 be the optimal spacing between the two nearest-neighbor binding sites, when the electrostatic interaction is "turned off" or screened sufficiently by the presence of a large amount of salt ions. Then a_0 is determined by the balance between headgroup repulsion and hydrocarbon-tail attraction. A reasonable choice is $a_0 = 8\,$Å, considering the typical cross-sectional area of LPS Re $\approx 166\,$Å^2[24]. We first calculate $F_{\rm elec}$ at a_0 and $a_0 + \delta a$. Then the electrostatic lateral pressure can be obtained as $\Delta\Pi = -\frac{1}{\delta a}\left[F_{\rm elec}(a_0+\delta a) - F_{\rm elec}(a_0)\right]$. As long as $\delta a \ll a_0$, $\Delta\Pi$ will not be sensitive to the choice of δa.

3.1 Effects of Mg^{2+} and cationic AMPs

In Fig. 5(a)-(d), we have displayed our results for $\Delta\Pi$, which show how the LPS layer can be modified electrostatically by Mg^{2+} and AMPs. Here [...] denotes the molar concentration of species .... (a) When $[Mg^+] = 0$, $\Delta\Pi$ is positive (outward) in the entire range of $[Na^+]$ shown, because of the repulsion between LPS charges. It is worth mentioning that this is more entropically driven[35]: by expanding the layer, some of bound ions are freed or they are more loosely bound. At higher $[Mg^+]$, $\Delta\Pi$ becomes negative (inward), more so for larger $[Mg^{2+}]$. For $[Mg^{2+}] = 1\,$mM, this effect tightens the LPS leaflet over a wide $[Na^+]$ range. ¶ The increase of $\Delta\Pi$ with increasing $[Na^+]$ in this case is a combined effect of reduced Mg^{2+} binding ‖ and screening of lateral interactions at higher $[Na^+]$. For too small $[Mg^{2+}]$ ($\approx 0,10\,\mu$M), however, $\Delta\Pi$ is a non-monotonic function of $[Na^+]$. In this case, it is mainly Na^+ that binds to the LPS layer. The entropic gain of freed Na^+ ions is less pronounced for larger $[Na^+]$. On the other hand, $\Delta\Pi$ tends to zero as $Na^+ \to 0$, since N_1 per area is roughly independent of a in that case. ** This explains the aforementioned non-monotonicity.

On the other hand, Fig. 5(b) shows the adverse effects of AMPs for given $Mg^{2+} = 0.1\,$mM. As [AMP] increases, the $\Delta\Pi$ curves shift upwards so that $\Delta\Pi$ becomes positive for larger [AMP]. This can be attributed to a reduced amount of bound Mg^{2+} at higher [AMP]. As [AMP] increases, AMPs continue to displace bound Mg^{2+} ions from the LPS layer, diminishing the tightening effect of these ions. It is worth noting that the individual charged residues of the AMP are monovalent, each neutralizing one LPS charge, similarly to what Na^+ does.

The results in Fig. 5(c) show the Mg^{2+}-tightening effect as a function of $[Mg^{2+}]$ for various choices of [AMP] and $[Na^+] = 100\,$mM. For given [AMP], this effect becomes stronger at higher $[Mg^{2+}]$, since the LPS layer becomes more populated with Mg^{2+}, which induces a negative lateral pressure. The tightening effect is less effective for larger [AMP]. Conversely speaking, the adverse effect of AMPs seen in Fig. 5(b) can be restored by increasing $[Mg^{2+}]$. As $[Mg^{2+}]$ increases, the amount of bound AMPs will diminish; higher $[Mg^{2+}]$ is required for higher [AMP]. Note that the curve for $[AMP] = 1\,\mu$M appears to be flat for $[Mg^{2+}] < 0.8\,$mM. A plausible reason is that in this case the LPS layer is mainly populated with AMPs (see Fig. 6). This is partly responsible for the observed insensitivity of $\Delta\Pi$ to Mg^{2+}.

The graph in Fig. 5(d) shows how the LPS-stabilizing ef-

§ The relationship between δ and r is not so obvious, if there is any. If hydration and ion binding influence both, ion binding on the LPS layer can reduce δ. This explain why $\delta < r$. Our choices of δ and r are typical ones[40].

¶ The Poisson-Boltzmann approach suggests that in a mixture of 100 mM monovalent ions and a few mM of divalent ions, divalent ions can preferentially bind to a highly-charged surface[40]. This is reflected in our results in Fig. 5(a).

‖ A quantitative picture of ion binding, especially the competitive binding between Mg^{2+} and AMPs, is presented in Fig. 6. Qualitatively speaking, the chemical potential of ion species (e.g., Mg^{2+}) increases, as their bulk concentration increases. This promotes the binding of these ions on the LPS layer.

** The easiest way to see this is to consider ion binding at the meanfield level, which works well in the low-salt limit. In this case, the effective planar charge density can be approximated as $-e\kappa/\pi\ell_B$, which is independent of a[41].

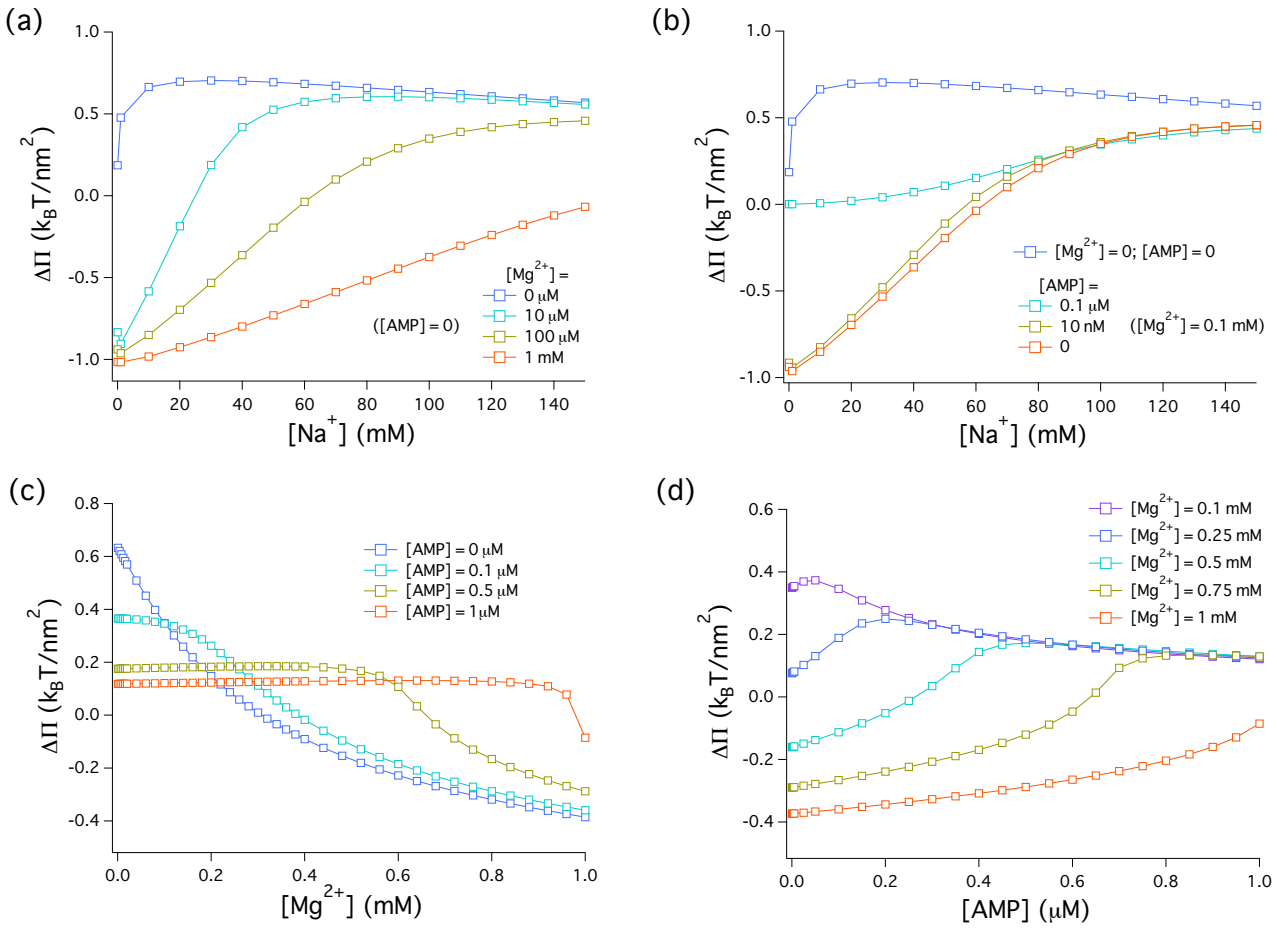

Fig. 5 Competing effects of Mg^{2+} and AMPs on the LPS layer. Here, [...] is the molar concentration of species ... (a) Mg^{2+}-tightening of the LPS layer. When $[Mg^{+}] = 0$, $\Delta\Pi$ is positive (outward) in the entire range of $[Na^{+}]$ shown. At higher $[Mg^{+}]$, $\Delta\Pi$ becomes negative (inward) over a large $[Na^{+}]$-range, more so for larger $[Mg^{2+}]$, indicating that Mg^{2+} tightens and stabilizes the LPS leaflet reliably. (b) Adverse effects of AMPs. As [AMP] increases, $\Delta\Pi$ shifts upwards. Similarly to the results in (a), the difference between various cases diminishes as $[Na^{+}]$ increases. (c) The adverse effect of AMPs can be counterbalanced by increasing $[Mg^{2+}]$. For this, higher $[Mg^{2+}]$ is needed for higher [AMP]. (d) Conversely, the LPS-stabilizing electrostatic effect of Mg^{2+} can be reversed by increasing [AMP].

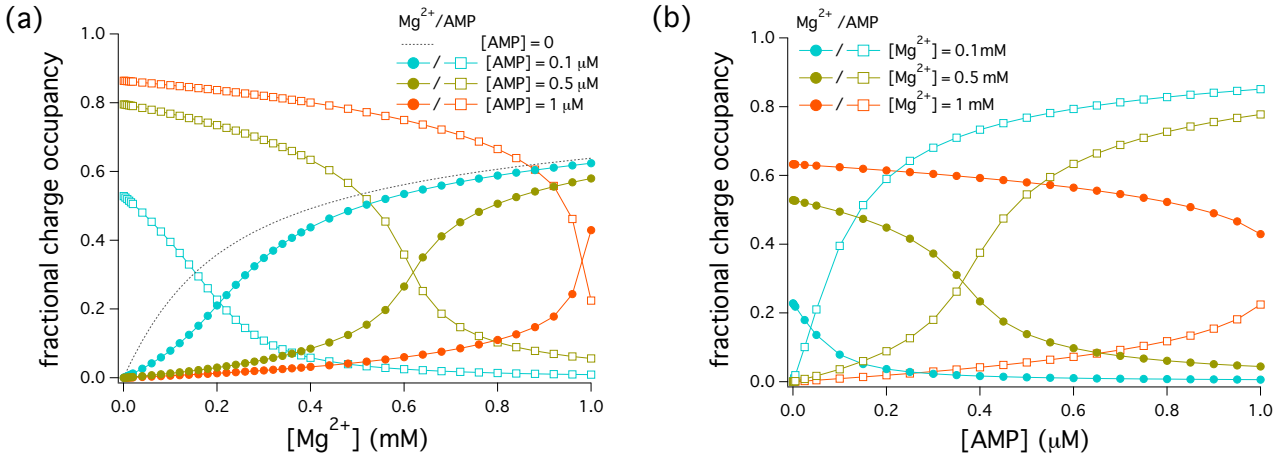

Fig. 6 Fractional (charge) occupancy of Mg^{2+} and AMPs on the LPS layer, $2N_2/N_0$ and QN_p/N_0, respectively. (a) As $[Mg^{2+}]$ increases, the occupancy of Mg^{2+} (AMPs) on the LPS layer increases (decreases). (b) On the other hand, as [AMP] increases, the occupancy of Mg^{2+} (AMPs) on the LPS layer decreases (increases). The behavior observed in Fig. 5 combines this effect.

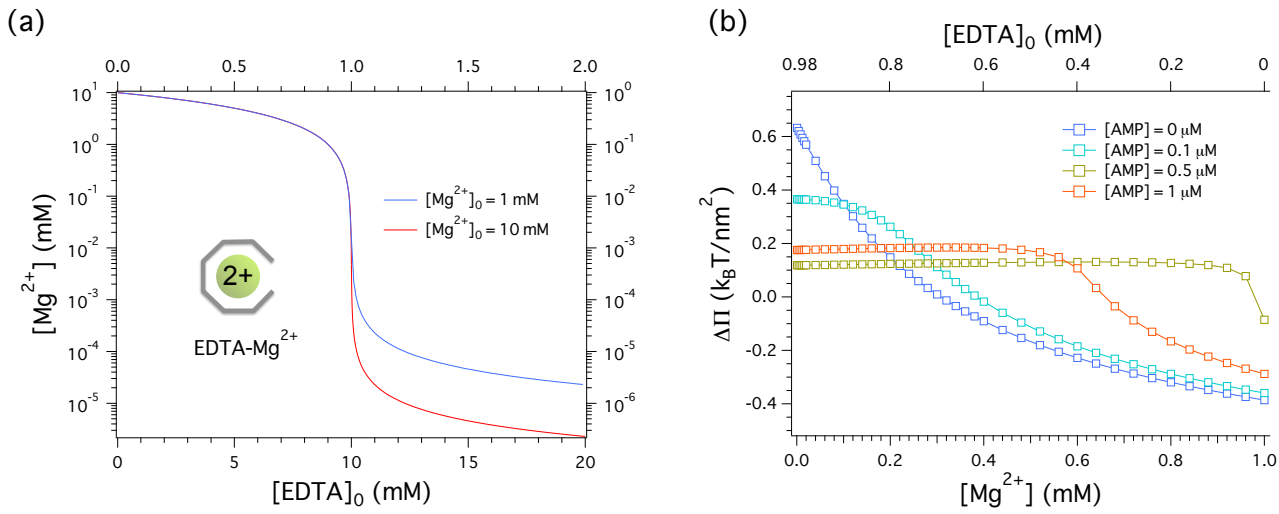

Fig. 7 (a) Mg^{2+} depletion via the reaction: $Mg^{2+} + \mathrm{EDTA} \leftrightarrow Mg^{2+} \cdot \mathrm{EDTA}$. The left-bottom axes correspond to $[Mg^{2+}]_0 = 10\,\mathrm{mM}$ and the right-top axes correspond to $[Mg^{2+}]_0 = 1\,\mathrm{mM}$. As $[\mathrm{EDTA}]_0$ increases, $[Mg^{2+}]$ decreases in solution, lowering the chemical potential of Mg^{2+} in bulk. As a result, some of Mg^{2+} ions bound to the LPS layer will be released, destabilizing the LPS layer. (b) EDTA and the lateral pressure. The lateral pressure graph in Fig 5(c) is recaptured as a function of $[\mathrm{EDTA}]_0$ (top axis). This shows how $\Delta\Pi$ changes as a function of $[\mathrm{EDTA}]_0$, when $[Mg^{2+}]_0 = 1\,\mathrm{mM}$. The top axis is constructed so that $[Mg^{2+}]$ on the bottom axis is the free Mg^{2+} concentration for a given $[\mathrm{EDTA}]_0$, as also described by the graph on the left; for instance, $[\mathrm{ETPA}]_0 = 0.2\,\mathrm{mM}$ corresponds to $[Mg^{2+}] \approx 0.8\,\mathrm{mM}$, and $[\mathrm{EDTA}]_0 = 0.98\,\mathrm{mM}$ to $[Mg^{2+}] \approx 0.02\,\mathrm{mM}$. In all cases shown, as $[\mathrm{EDTA}]_0$ increases, $\Delta\Pi$ becomes positive.

fect of Mg^{2+} seen in (c) can be reversed by increasing [AMP]. For larger $[Mg^{2+}]$, larger [AMP] is required to counteract the favorable effect of Mg^{2+}.

The Mg^{2+}-tightening effect demonstrated in Fig. 5, especially in (c), is consistent with a series of experimental observations such as diminished water penetration through LPS layers or decreased LPS chain mobility, in the presence of divalent cations[20–22,25]. It is worth noting that electrostatic modification of LPS headgroups is responsible for these observations. In our approach, it is qualified in terms of $\Delta\Pi$, the electrostatic contribution to the lateral pressure in the plane of headgroups. Importantly, it is well aligned with the view of divalent cations as OM-stabilizing agents, which increase bacterial resistance against cationic AMPs or other membrane-perturbing agents[3–13].

Our results presented in Fig. 5 reflect the electrostatic interactions occurring on the LPS layer. These effects are, however, influenced by the competitive binding of charged objects. Fig. 6 displays our results for the fractional (charge) occupancy of Mg^{2+} and AMPs on the LPS layer (for $[Na^+] = 100\,\mathrm{mM}$): $2N_2/N_0$ (filled circles) and QN_p/N_0 (unfilled squares). (a) As $[Mg^{2+}]$ increases, the occupancy of Mg^{2+} (AMPs) on the LPS layer increases (decreases). This finding is consistent with experimental observations (with different molecules) in Refs.[3–5]. At higher [AMP], higher $[Mg^{2+}]$ is needed to displace effectively AMPs from the LPS layer. (b) On the other hand, as [AMP] increases, the occupancy AMPs (Mg^{2+}) on the LPS layer increases (decreases). At higher $[Mg^{2+}]$, higher [AMP] is required to displace Mg^{2+} ions from the LPS layer. The behavior observed in (a)-(c) combines this effect and electrostatic interactions on the LPS layer.

3.2 Effects of EDTA

Ethylene-diaminetetraacetic acid (EDTA) is polyanionic (typically carrying four negative charges) and can sequester metal cations such as Mg^{2+} or Fe^{3+}. EDTA-Mg^{2+} complexation can be described by the simple reaction:

$$K = \frac{[\mathrm{Mg}^{2+}\cdot\mathrm{EDTA}]}{[\mathrm{Mg}^{2+}][\mathrm{EDTA}]} = \frac{[\mathrm{Mg}^{2+}\cdot\mathrm{EDTA}]}{\left([\mathrm{Mg}^{2+}]_0 - [\mathrm{Mg}^{2+}\cdot\mathrm{EDTA}]\right)\left([\mathrm{EDTA}]_0 - [\mathrm{Mg}^{2+}\cdot\mathrm{EDTA}]\right)}, \tag{16}$$

where $[...]_0$ is the initial concentration of species ... (K in this equation is not to be confused with K in Eq. 2). This equation explains how Mg^{2+} is depleted from the solution as $[\mathrm{EDTA}]_0$ increases. Adding EDTA molecules is equivalent to reducing $[Mg^{2+}]$.

Fig. 7(a) shows our results for $[Mg^{2+}]$ as a function of $[\mathrm{EDTA}]_0$. For this, we used $\log_{10} K \approx 8.64$[42]. If the left-bottom axes correspond to $[Mg^{2+}]_0 = 10\,\mathrm{mM}$, the right-top axes correspond to $[Mg^{2+}]_0 = 1\,\mathrm{mM}$. As $[\mathrm{EDTA}]_0$ increases, $[Mg^{2+}]$ decreases in bulk via the reaction in Eq. 16. This will lower the chemical potential of free Mg^{2+} ions. As a result, some of previously-bound Mg^{2+} ions will be released from the LPS layer.

In Fig. 7(b), we have recaptured Fig. 5(c) to show how the lateral pressure varies as EDTA continues to deplete Mg^{2+} (top axis). For this, the initial free Mg^{2+} concentration is chosen to be $[Mg^{2+}]_0 = 1\,\mathrm{mM}$. Also the top and bottom axes vertically correspond to each other with the bottom axis describing the concentration of free Mg^{2+} ions. For instance, $[\mathrm{ETPA}]_0 = 0.2\,\mathrm{mM}$ corresponds to $[Mg^{2+}] \approx 0.8\,\mathrm{mM}$, and $[\mathrm{EDTA}]_0 = 0.98\,\mathrm{mM}$ to $[Mg^{2+}] \approx 0.02\,\mathrm{mM}$. In all cases shown, as $[\mathrm{EDTA}]_0$ increases, $\Delta\Pi$ becomes (more) positive; it changes sign at lower $[\mathrm{EDTA}]_0$ (in the low milli-molar range) at higher [AMP].

The results in Fig. 7 offer a quantitative picture of how EDTA can perturb the LPS layer and the OM[3,4,8,9]. They are also well aligned with the observation of EDTA-induced LPS release from the LPS layer into the solution. In the presence of EDTA, individual LPS headgroups are swollen by the repulsion between their negative changes ($\Delta\Pi > 0$). This creates a mismatch in the optimal areas of the inner and outer layers. The resulting unfavourable stress can be relieved by LPS release. Because of the coarse-grained nature of our model, however, it may to be used to understand the varying degree of LPS release by different agents[3,4,8,9].

4 Conclusion

As its distinguishing design feature, the bacterial outer membrane (OM) is highly asymmetrical with its outer layer mainly consisting of LPS (lipopolysaccharide) molecules[1–5]. Each LPS molecule is polyanionic; for instance, LPS Re typically carries four negative changes in an aqueous solution. Nominally, the OM is a remarkable permeability barrier. However the polyanionic nature of LPS is implicated in OM permeability. Indeed, the LPS layer (thus the OM) can be elec-

trostatically modified[3–13]. At the heart of this is the cation-binding ability of LPS, which can bring about competing effects on the LPS layer first and then the OM as a whole. A commonly-accepted view is that if Mg^{2+} is an OM stabilizing agent, plolycationic AMPs or polyanionic EDTA is an OM perturbing agent[3–13].

In this work, we have developed a coarse-grained model for describing how the LPS layer can be modified electrostatically, especially by Mg^{2+}, EDTA, and AMPs or polycations (e.g., magainin 2). In our model, LPS charges are assumed to be arranged on a two-dimensional square lattice. While it is suitable for the simplest form of LPS, i.e., LPS Re, the general feature of our findings may remain relevant for other LPS molecules, since the electrostatic effects we focus on are rather generic and are not sensitive to such molecular details. On the other hand, our model captures a few key features of the LPS system or a highly-charged surface such as charge discreteness, ion pairing on LPS, and lateral correlations between an Mg^{2+}-backbone charge pair and unpaired backbone charges. In the absence of amphiphilic molecules (e.g., AMPs), our approach allows one to examine systematically electrostatic modification of the LPS layer; or it will help clarify the role of electrostatic effects in altering OM permeability.

Other details can be added as we understand better how they fit into our model. For instance, the hydrophobic interaction of AMPs with the LPS layer can be incorporated into our electrostatic picture, similar to what was done for a phospholipid membrane[33]. Such an effort will rely on the availability of a free-energy model for describing the hydrophobic insertion of AMPs into the LPS layer. Also the asymmetric lipid distribution between the two layers of the OM is expected to be implicated in OM permeability. The permeability of a membrane bilayer can be regulated independently by the two layers[29]. This may justify the neglect of lipid asymmetry, and one can focus on the LPS layer or LPS bilayers[16,19,20]. Thus extended efforts along the lines of our discussions here will be useful for developing a more realistic model of OM permeability.

Our results can be summarized as follows. At their physiological concentrations (μM for AMP^{4+} and mM for Mg^{2+}), these polycations effectively modify the LPS layer electrostatically: while Mg^{2+} tightens and stabilizes the LPS layer, AMPs or EDTA counteracts this favorable effect by displacing previously-bound Mg^{2+} ions from the LPS layer competitively or by depleting Mg^{2+} from the solution, respectively. Our approach offers a quantitative basis for the long-standing observation of Mg^{2+}-AMP-EDTA dependent permeability of the outer membrane of Gram-negative bacteria[3–13] or LPS membranes[19–22].

Our results clearly show how Mg^{2+} tightens the LPS layer at a milli-molar range. This effect is a result of its preferential binding and lateral-charge correlations it induces. (Recall the relevant footnote in Sec. 3.) This leads to charge inhomogeneity on the LPS surface, even at a small concentration of Mg^{2+}: it inverts locally the sign of charge on the binding site, turning an otherwise repulsive interaction between adjacent sites into an attraction. This is responsible for Mg^{2+}-tightening of the LPS layer, which has long been appreciated in the literature[3–13,19–22] but is quantified in this work in terms of a negative excess lateral pressure (Fig. 5).

Similar electrostatic effects govern a few related phenomena. For instance, it was observed that divalent cations diminish water penetration through LPS layers or decrease LPS chain mobility[20,21]; or they induce LPS lipid-tail ordering[2,3]. What underlies all these is the ability of divalent cations to create a negative lateral pressure in the plane of lipid headgroups (See Fig. 5).

AMPs are amphiphilic molecules, often viewed as 'pore formers' in the bacterial cell surface[13] (see Refs.[12,13] for more details as well as for alternative views on their microbial killing mechanism). In our model, a polycationic peptide is modelled as a linear array of a few charges Q. When $Q = 4$ as for magainin 2,[12] our results in Fig. 5 indicate that a low micro-molar range of AMPs is required for counterbalancing Mg^{2+} effects. The MIC (minimal inhibitory concentration) of magainin 2[13,43,44], i.e., the minimum concentration at which a given AMP is effective against a particular strain of bacteria[44], falls in the low micro-molar range. It is worth noting that MICs also depend on cell concentrations used, since the cell concentration dictates the competition of cells to bind AMPs[43]. Also, according to our results in Fig. 6, the presence of Mg^{2+} can influence the MIC, because of its electrostatic competition with cationic AMPs for an oppositely-charged membrane; in the presence of Mg^{2+}, a larger AMP concentration is needed to reach a high enough coverage on the membrane surface so as to permeabilize the membrane. On the other hand, as it is, our approach is suitable for a single infinite LPS layer. Thus these AMP concentrations should not be taken literally. Nevertheless, our observation tends to suggest that once AMPs overcome the permeability barrier of the bacterial outer membrane, they can reach and perturb the cytoplasmic membrane in the same or similar concentration range.

Our approach can be extended to study how AMPs are partitioned between the outer and inner membranes of Gram-negative bacteria, advancing our understanding of the role of the outer membrane in neutralizing AMP's activity. Cell selectivity experiments with vesicle membranes, mimicking the inner membrane, will inevitably overestimate the selectivity for the bacterial membrane, if not corrected for the trapping of AMPs in the outer membrane, especially in the LPS layer[12] (also see Refs.[13,43] for AMP interactions with LPS). Further considerations along this line will thus be beneficial for clarifying better AMP's cell selectivity[43] for microbial vs. host cell membranes.

Acknowledgment

This work was supported by NSERC (Canada) (B.-Y.H.). One of us (B.Y.H.) acknowledges useful discussions with R. R. Farzami and S. Taheri-Araghi.

Appendix

In this Appendix, we derive a few key theoretical results presented in the main text, especially in Eq. 6. While some of them are discussed in the literature[27,28,45], we not only reproduce them here in a more coherent way but also extend them to the LPS system.

A. Homogeneous lattice

Let us begin with a fully-charged, homogeneous lattice with a lattice constant a, consisting of N_0 lattice sites; each lattice site is occupied by a charge of valence Z. The total electrostatic energy is given by a sum over all distinct pairs of charges at $\mathbf{r}_i$ of screened Coulomb interactions: $V_{ij}/k_BT = \Delta\ell_B e^{-\kappa|\mathbf{r}_i-\mathbf{r}_j|}/|\mathbf{r}_i-\mathbf{r}_j|$. Recall that Δ accounts for the dielectric property of LPS: $\Delta \approx 2$ near or inside LPS and $\Delta = 1$ in water. It proves useful to introduce the pair interaction E_{nm} per site between two charges separated by (na, ma) (n-lattice sites apart in the x direction and m-lattice sites in the y direction). With the convention $k_BT = 1$, E_{nm} is given by

$$E_{nm}\cdot N_0 = Z^2\Delta\ell_B\left(\frac{N_0}{A}\right)^2\int\int_{R_{nm}} d^2r d^2r' \frac{e^{-\kappa\mathbf{r}-\mathbf{r}'}}{|\mathbf{r}-\mathbf{r}'|}, \tag{A-1}$$

where A is the total area of the lattice and

$$R_{nm} = \left\{\left(n-\tfrac{1}{2}\right)a < x-x' < \left(n+\tfrac{1}{2}\right)a, \left(m-\tfrac{1}{2}\right)a < y-y' < \left(m+\tfrac{1}{2}\right)a\right\}. \tag{A-2}$$

If L be the length of the entire lattice, assumed to be square, $A = L^2$ and $N_0 = L^2/a^2$. Each integral in (A-1) runs from $-L/2$ to $L/2$. To avoid "edge effects," we let $L \to \infty$.

The x-x' integrals in Eq. (A-1), for instance, are to be carried out over a stripe in the diagonal direction in the x-x' plane. Hence the change of variables $X' = \frac{x+x'}{\sqrt{2}}$, $X'' = \frac{x-x'}{\sqrt{2}}$ transforms the integration domain into a vertical stripe, with X' running from $\frac{-L}{\sqrt{2}}$ to $\frac{L}{\sqrt{2}}$ and X'' from $\frac{(n-1/2)a}{\sqrt{2}}$ to $\frac{(n+1/2)a}{\sqrt{2}}$. Also, this is an orthonormal transformation with the jacobian equal to 1. With similar transformation with other integration variables, we find

$$\begin{aligned} E_{nm} &= Z^2\Delta\ell_B\left(\frac{N_0}{A^2}\right)\int_{-L/\sqrt{2}}^{L/\sqrt{2}}dX'\int_{-L/\sqrt{2}}^{L/\sqrt{2}}dY'\int_{(n-1/2)a/\sqrt{2}}^{(n+1/2)a/\sqrt{2}}dX''\int_{(m-1/2)a/\sqrt{2}}^{(m+1/2)a/\sqrt{2}}dY''\frac{\exp(-\kappa\sqrt{2(X''^2+Y''^2)})}{\sqrt{2(X''^2+Y''^2)}} \\ &= 2Z^2\Delta\ell_B\left(\frac{N_0}{A}\right)\int_{(n-1/2)a/\sqrt{2}}^{(n+1/2)a/\sqrt{2}}dX''\int_{(m-1/2)a/\sqrt{2}}^{(m+1/2)a/\sqrt{2}}dY''\frac{\exp(-\kappa\sqrt{2(X''^2+Y''^2)})}{\sqrt{2(X''^2+Y''^2)}} \\ &= \frac{Z^2\Delta\ell_B}{a^2}\int_{(n-1/2)a}^{(n+1/2)a}dX\int_{(m-1/2)a}^{(m+1/2)a}dY\frac{\exp(-\kappa\sqrt{X^2+Y^2})}{\sqrt{X^2+Y^2}}. \end{aligned} \tag{A-3}$$

In the last step, we used $X = \sqrt{2}X'' = (x-x')$ and $Y = \sqrt{2}Y'' = (y-y')$.

Let Σ and Σ_1 denote the mean field energy per site, including and excluding the self-energy contribution, i.e., the interaction within the same site, respectively:

$$\Sigma = \sum_{n=-\infty}^{\infty}\sum_{m=-\infty}^{\infty}E_{nm} \text{ and } \Sigma_1 = \Sigma - E_{00}. \tag{A-4}$$

The total energy of the lattice is then $\frac{N_0}{2}\Sigma$ or $\frac{N_0}{2}\Sigma_1$, depending on whether to include the self-energy or not; the factor $\frac{1}{2}$ is introduced to avoid double counting.

By converting the sum into a corresponding integral, we find

$$\begin{aligned} \Sigma &= \frac{Z^2\Delta\ell_B}{a^2}\int_{-\infty}^{\infty}dX\int_{-\infty}^{\infty}dY\frac{\exp(-\kappa\sqrt{X^2+Y^2})}{\sqrt{X^2+Y^2}} \\ &= \frac{Z^2\Delta\ell_B}{a^2}\frac{2\pi}{\kappa} \end{aligned} \tag{A-5}$$

and

$$\Sigma_1 = \Sigma - E_{00} = \frac{Z^2\Delta\ell_B}{a^2}\left(\frac{2\pi}{\kappa} - \mathscr{M}_1\right). \quad \text{(A-6)}$$

Note here that $E_{00} = \frac{Z^2\Delta\ell_B}{a^2}\mathscr{M}_1$ denotes the self-energy of each square lattice site and $\mathscr{M}_1$ is given by

$$\mathscr{M}_1 = \int_{-a/2}^{a/2} dX \int_{-a/2}^{a/2} dY \frac{\exp(-\kappa\sqrt{X^2+Y^2})}{\sqrt{X^2+Y^2}}. \quad \text{(A-7)}$$

For a later convenience, it is useful to combine ν successive squares into a rectangle. The interaction energy between the rectangle and the rest on the lattice denoted as Σ_ν is given by Σ minus the contribution of the rectangle (including self-interactions of the squares). Similarly to those shown above, we obtain

$$\Sigma_\nu = \frac{Z^2\Delta\ell_B}{a^2}\left(\frac{2\pi}{\kappa} - \mathscr{M}_\nu\right). \quad \text{(A-8)}$$

where $\mathscr{M}_\nu$ is given by

$$\mathscr{M}_\nu = \int_{-\nu a/2}^{\nu a/2} dX \int_{-a/2}^{a/2} dY \frac{\exp(-\kappa\sqrt{X^2+Y^2})}{\sqrt{X^2+Y^2}}. \quad \text{(A-9)}$$

This includes $\mathscr{M}_1$ in Eq. (A-7) as a special case.

In summary, the total electrostatic free energy of the homogeneous lattice, excluding self-energy, is

$$F_{\rm elec} = \frac{N_0}{2}\Sigma_1. \quad \text{(A-10)}$$

B. Homogeneous lattice with "holes"

Imagine removing M charges from an otherwise perfect lattice introduced in Subsec. A of this appendix, leaving $N = N_0 - M$ charges on the lattice. The total energy of such an "irregular" lattice or a homogeneous lattice with "holes" is equal to the total energy of the original homogeneous lattice ($\frac{N_0}{2}\Sigma_1$) − the energy between each removed charge and the rest ($M\Sigma_1$) + the energy among the removed charges (denoted as F_{rr}). Hence we have [††]

$$F_{\rm elec} = \frac{N_0}{2}\Sigma_1 - M\Sigma_1 + F_{rr}. \quad \text{(B-1)}$$

Obviously, F_{rr} depends on the relative positions of the removed charges. However, for $M \gg 1$, we can approximate it as its average over all possible configurations of the removed charges. Within this simplification, F_{rr} is just the energy of a homogeneous lattice with a reduced planar density M/N_0.

$$F_{rr} \approx \frac{M^2}{N_0}\frac{\Sigma_1}{2}. \quad \text{(B-3)}$$

For $M = N_0$, this reduces to the energy of the original homogeneous lattice.

Hence the total electrostatic energy is given by

$$\begin{aligned} F_{\rm elec} &\approx \frac{N_0}{2}\Sigma_1 - M\Sigma_1 + \frac{1}{2}\frac{M^2}{N_0}\Sigma_1 \\ &= \frac{N^2}{N_0}\frac{\Sigma_1}{2}. \end{aligned} \quad \text{(B-4)}$$

This is identical to the energy of N ions uniformly distributed on the lattice of N_0 sites. We can also include self-energies of the lattice sites by replacing Σ_1 by Σ. For a homogeneous lattice with holes, Eq. (B-1) appears to be a detour to Eq. (B-4) at best. But this will be useful for an inhomogeneous lattice.

In principle, we can use the same method to calculate the interaction energy between two *different* types of particles on a lattice. The resulting electrostatic energy will be given by

$$F_{\rm elec} = \frac{(Z_iN_i)(Z_jN_j)}{N_0}\frac{\Sigma_i + \Sigma_j}{2}. \quad \text{(B-5)}$$

Between small ions (e.g., Na^+ or Mg^{2+}), $\Sigma_i = \Sigma_j = \Sigma_1$. Then Eq. (B-5) is a straightforward generalization of Eq. (B-4). But for peptide-ion interactions, $\frac{\Sigma_i+\Sigma_j}{2} = \frac{\Sigma_1+\Sigma_\nu}{2}$. Depending on whether we smear out ion or peptide charges, while keeping the other discrete, the interaction energy contains Σ_1 or Σ_ν, respectively. The combination in Eq. (B-5) can be considered as an average over these two possibilities.

Note that $F_{\rm elec}$ in this subsection and in the last subsection is the meanfield free energy $F_{\rm MF}$.

C. Lateral correlations

Unlike the meanfield energy term in Eq. (A-10) or Eq. (B-4) or the transverse interaction in Eq. (D-4) in the next subsection, the lateral-interaction free energy is less obvious to construct. Here we will present one, which is accurate for the two limiting cases: a homogeneously-charged lattice treated in Subsec. B and a perfect, alternating lattice, where the sign of charge alternates without any hole as illustrated in Fig. 4 (see the lattice labelled as (i)).

Imagine distributing N_+ positive charges and N_- negative charges on an otherwise empty lattice with N_0 sites, leaving $M = N_0 - N_+ - N_-$ sites unoccupied. The free energy of this charge distribution can be calculated similarly to the procedure adopted in Subsec. B. The reference state we start from

[††] To see this, suppose we have a collection of changes labelled as 1, 2, 3, ... Recall that V_{ij} is the interaction energy between charges i and j. If $W(k,l,m)$ is the work required to remove charges k, l, and m, it is given by

$$\begin{aligned} W(k,l,m) &= -\textstyle\sum_j V_{kj} - \sum_{j\neq k} V_{lj} - \sum_{j\neq k,l} V_{mj} \\ &= -\textstyle\sum_j V_{kj} - \sum_j V_{lj} - \sum_j V_{mj} + (V_{lk} + V_{mk} + V_{ml}) \\ &= -M\times\Sigma + F_{rr}, \quad (M=3). \end{aligned}$$

If self-energy is omitted, Σ should be replaced by Σ_1. The total free energy stored, excluding self-energy, is then $F_{\rm elec} = \frac{1}{2}N_0\Sigma_1 + W(l,m,k)$. This is a special case of Eq. (B-1). Also note that the last equality holds for an infinite plane whether uniformly or alternatively charged (see Eq. (C-3)).

is a perfect, fully occupied alternating lattice: $N_+ = N_- = \frac{1}{2}N_0$ and $M = 0$. The resulting free energy is given by

$$F_{\rm elec} = \frac{N_0}{2}\Sigma_{\rm alt}. \qquad \text{(C-1)},$$

where $\Sigma_{\rm alt}$ describes the interaction between a charge and all the other charges:

$$\Sigma_{\rm alt} = \sum_{n=-\infty}^{\infty}\sum_{\substack{m=-\infty \\ (n,m)\neq(0,0)}}^{\infty}(-1)^{n+m}E_{nm}, \qquad \text{(C-2)}$$

where E_{nm} is defined in Eq. (A-3) (with $Z = 1$).

The electric free energy can then be obtained by simply removing charges (both positive and negative) from the perfect lattice:

$$F_{\rm elec} = \frac{N_0}{2}\Sigma_{\rm alt} - M\Sigma_{\rm alt} + F_{rr}. \qquad \text{(C-3)}$$

The first term is the energy of the perfect lattice, the second term is the energy between each removed charge and all the other charges, while the last term is the energy among the removed charges (in units of k_BT).

The term F_{rr} in Eq. (C-3) is determined by three contributions of removed charges: (i) the interaction among positive charges (green balls in Fig. 4), (ii) the interaction among negative charges (tangerine balls in Fig. 4), and (iii) the interaction among positive and negative charges (coupling between green and tangerine balls), all removed from the lattice. For two charges separated by (na, ma), their interaction is repulsive if $n+m$ is even and attractive if $n+m$ is odd. We thus introduce $\Sigma_{\rm odd}$ and $\Sigma_{\rm even}$ defined as

$$\Sigma_{\rm odd} = \sum_{n=-\infty}^{\infty}\sum_{\substack{m=-\infty \\ (n,m)\neq(0,0) \\ n+m\ \text{odd}}}^{\infty}E_{nm} \quad \text{and} \quad \Sigma_{\rm even} = \sum_{n=-\infty}^{\infty}\sum_{\substack{m=-\infty \\ (n,m)\neq(0,0) \\ n+m\ \text{even}}}^{\infty}E_{nm} \qquad \text{(C-4)}$$

Obviously, $\Sigma_{\rm odd}$ corresponds to the interaction among all opposite-charge pairs, while $\Sigma_{\rm even}$ represents the interaction among all like charges. Also, note that

$$\Sigma_{\rm alt} = \Sigma_{\rm even} - \Sigma_{\rm odd} \ \text{ and } \ \Sigma_1 = \Sigma_{\rm even} + \Sigma_{\rm odd}. \qquad \text{(C-5)}$$

Using a method similar to the one that leads to Eq. (B-3), we calculate the energy among the removed charges:

$$\begin{aligned} F_{rr} &= \frac{1}{N_0}\left(\frac{N_0}{2}-N_+\right)^2\Sigma_{\rm even} + \frac{1}{N_0}\left(\frac{N_0}{2}-N_-\right)^2\Sigma_{\rm even} - \frac{2}{N_0}\left(\frac{N_0}{2}-N_+\right)\left(\frac{N_0}{2}-N_-\right)\Sigma_{\rm odd} \\ &= \frac{2}{N_0}\left(\frac{N_0}{2}-N_+\right)\left(\frac{N_0}{2}-N_-\right)\Sigma_{\rm alt} + \frac{(N_+-N_-)^2}{N_0}\Sigma_{\rm even}. \end{aligned} \qquad \text{(C-6)}$$

To understand the nature of approximations made here, consider the first term in the first line, for instance, that describes the repulsion between positive charges removed. An alternative choice is $\left(\frac{1}{2}N_0 - N_+\right)\cdot\Sigma_1\left(a\sqrt{N_0/\left(\frac{1}{2}N_0-N_+\right)}\right)$, which is the energy of $\left(\frac{1}{2}N_0 - N_+\right)$ charges on a "dilated" lattice of lattice constant $a_{\rm new} = a\sqrt{N_0/\left(\frac{1}{2}N_0-N_+\right)}$. Similarly, we can construct the interaction energy between opposite charges. The resulting F_{rr} will be different from the one in Eq. (C-6) unless $\kappa \to 0$; in the limit $\kappa \to 0$, the two converge onto each other, since the transformation of this dilated lattice back to the original one with a lattice constant a by some factor is equivalent to rescaling charge densities by the same factor. However, we note that it is more cumbersome to analyze such an expression numerically (see Eqs. 11 and 13), even though the difference between these two approximation schemes might be only a subtle one. More conceptually, the new lattice constant $a_{\rm new}$, which can be interpreted as the shortest distance between charges, varies with N_+/N_0. In reality, however, this distance is set by ionic or molecular sizes as assumed in our original picture. Below we argue that our final result is valid in the aforementioned limiting cases (a homogeneously-charged lattice and a perfect, alternating lattice). It is thus expected to interpolate the actual lateral free energy in the intermediate case.

If combined with F_{rr} in Eq. (C-6), $F_{\rm elec}$ in Eq. C-3 becomes

$$\begin{aligned} F_{\rm elec} &= \frac{N_0}{2}\Sigma_{\rm alt} - M\Sigma_{\rm alt} + \frac{2}{N_0}\left(\frac{N_0}{2}-N_+\right)\left(\frac{N_0}{2}-N_-\right)\Sigma_{\rm alt} + \frac{(N_+-N_-)^2}{N_0}\Sigma_{\rm even} \\ &= 2\frac{N_+N_-}{N_0}\Sigma_{\rm alt} + \frac{(N_+-N_-)^2}{N_0}\Sigma_{\rm even}. \end{aligned} \qquad \text{(C-7)}$$

If the second term in (C-7) is already accounted for in the mean field terms, the first term is the lateral correlation term:

$$F_{\rm LC} = 2\frac{N_+N_-}{N_0}\Sigma_{\rm alt}. \qquad \text{(C-8)}$$

Also for the system we consider, $N_+ = N_2$ and $N_- = N_0 - N_1 - N_2 - QN_p$. Thus we can rewrite $F_{\rm LC}$ as

$$F_{\rm LC} = -2\ell_B\Delta\frac{N_2(N_0-N_1-N_2-QN_p)}{N_0}\,\zeta. \qquad \text{(C-9)}$$

where ζ is an infinite sum given in Eq. 8:

$$\zeta = \frac{1}{2}\sum_{i=1}^{\infty}\sum_{j=0}^{i}(-1)^{i+j-1}\frac{e^{-\kappa a\sqrt{i^2+j^2}}}{a\sqrt{i^2+j^2}}\cdot k(i,j)$$

with $k(i,j)$ defined as

$$k(i,j) = \begin{cases} 4 & \text{if } j=0 \text{ or } i=j \\ 8 & \text{otherwise} \end{cases}.$$

The final results in Eq. (C-8) or Eq. (C-9) were obtained for $N_\pm \le \frac{1}{2}N_0$. On the other hand, we expect $F_{\rm LC}$ to reach its minimum for $N_+ = N_- = \frac{1}{2}N_0$ and to vanish if $N_+ = N_0$ or $N_- = N_0$ (meaning that $N_1 = N_p = 0$). This expectation is satisfied by $F_{\rm LC}$ in Eqs. (C-8) and (C-9). Accordingly, this term is not only accurate in the aforementioned limiting cases but also interpolates (at least approximately) the actual one in the intermediate parameter range.

D. Mean-field limit and charge discreteness

As illustrated earlier, any distribution of ions and peptides on a lattice can be broken down into a superposition of two lattices: an alternating lattice and a lattice with the net charge smeared-out. The alternating lattice is treated in the last subsection. Using Eq. (B-4), the (mean-field) free energy of the latter, including self-energy of lattice sites, can be readily obtained as

$$F_{\rm MF}\frac{N_0^2a^2}{\Delta\ell_B} = \frac{\pi}{\kappa}(N_0-N_1-2N_2-QN_p)^2. \qquad \text{(D-1)}$$

This continuum description has a few drawbacks, since it ignores charge discreteness. First, it becomes inaccurate for the energy estimate of individual sites that represent otherwise discrete charges (e.g., backbone charges or counterion charges). ‡‡ Also, in this consideration, different bound charges are allowed to overlap. Second, it ignores the "connectivity" of charges on a given peptide. To remedy these, we treat peptides as Q separate charges and then account for their connectivity. The obvious improvement is to remove self-energy of each lattice site (see Eq. (B-4)):

$$F_{\rm MF}\frac{N_0^2a^2}{\Delta\ell_B} = \left(\frac{\pi}{\kappa}-\frac{\mathscr{M}_1}{2}\right)(N_0-N_1-2N_2-QN_p)^2. \qquad \text{(D-2)}$$

The term containing $\mathscr{M}_1$ is the self-energy of each lattice site.

Because of charge connectivity of a peptide, the self-energy correction made in Eq. (D-2) is not accurate for peptide-peptide interactions and peptide-ion interactions. The correct self-energy correction for the former interaction should read $-\frac{\mathscr{M}_p}{2}(QN_p)^2$. This issue is more subtle for the latter interaction. If we consider an ion interacting with peptide charges smeared out, we would use $-\mathscr{M}_1(QN_p)(N_1+2N_2)$ as a correction. On the other hand, if we focus on a peptide interacting with ions smeared out, $-\mathscr{M}_p(QN_p)(N_1+2N_2)$ is the correct correction term. To circumvent this subtlety, we use the average $-\frac{\mathscr{M}_p+\mathscr{M}_1}{2}(QN_p)(N_1+2N_2)$. This line of reasoning leads to

$$\begin{aligned} F_{\rm MF}\frac{N_0^2a^2}{\Delta\ell_B} &= \left(\frac{\pi}{\kappa}-\frac{\mathscr{M}_1}{2}\right)(N_0-N_1-2N_2-QN_p)^2 \\ &\quad -\frac{\mathscr{M}_p-\mathscr{M}_1}{2}QN_p(N_1+2N_2+QN_p). \end{aligned} \qquad \text{(D-3)}$$

The transverse interaction between a backbone charge and a bound charge (Fig. 1) is omitted in Eqs. (D-1)-(D-3). This effect can readily be obtained as[27]

$$-N_i\ell_B\Delta\left(\frac{Z_i}{\delta_i}\right) \text{ and } -N_p\ell_B\Delta\left(\frac{Q}{\delta_p}\right). \qquad \text{(D-4)}$$

Here δ_i is the distance between the paired opposite charges.

A related effect is the self-energy of counterions or peptide charges. If considered as charged spheres of radius δ_i, the self-energies of ions and peptides are, respectively, given by

$$N_i\Delta\ell_B\left(\frac{Z_i^2}{2\delta_i}\right) \text{ and } N_p\Delta\ell_B\left(\frac{Q}{2\delta_p}\right). \qquad \text{(D-5)}$$

Note that this energy changes as Δ varies. It thus influences binding on a dielectric surface. The self-energy of ions or AMPs in bulk with reference to the LPS surface becomes

$$\begin{aligned} &-N_i\frac{Z_i^2}{2}\frac{\ell_B}{\delta_i}(\Delta-1)-N_i\frac{Z_i^2}{2}\frac{\ell_B\kappa}{1+\kappa\delta_i}, \\ &-N_p\frac{Q}{2}\frac{\ell_B}{\delta_p}(\Delta-1)-N_p\frac{Q}{2}\frac{\ell_B\kappa}{1+\kappa\delta_p}. \end{aligned} \qquad \text{(D-6)}$$

In this expression, we included the polarization energy of ions in bulk: the change in the electrostatic free energy of an ion due to the surrounding ionic cloud, which can be obtained via

‡‡ Ion binding is not influenced by the self energy of individual backbone charges, which remains unchanged. The self-energy of ions changes near a dielectric medium (e.g., the LPS layer) and influences their affinity for the LPS layer. See the relevant discussion around Eq. (D-5).

the Debye charging process[37]. To obtain this for a peptide, we viewed it as being made of Q isolated charges, redistributing the surrounding ions. Note that this term is roughly an order of magnitude smaller than the first term and could be ignored. The corresponding effect on the LPS surface will not be included, since on the surface, ions will be more strongly correlated with the surrounding surface charges. Finally, we will not include the self-energy of backbone charges, since it is a constant and is independent of N_i and a.

In Eq. (D-6), the interaction between charges on the same peptide is not included. This extra energy can be readily obtained as $\Delta\ell_B\frac{\mathscr{M}_p-\mathscr{M}_1}{2a^2}$ on the LPS surface. In bulk, we can just set $\Delta=1$. Even though the peptide is more disordered in bulk, we do not take into account this feature.

The self-energy of a peptide in (D-6) thus becomes

$$-\frac{QN_p}{2}\ell_B(\Delta-1)\left(\frac{1}{\delta_p}+\frac{\mathscr{M}_p-\mathscr{M}_1}{a^2}\right)-\frac{QN_p}{2}\frac{\ell_B\kappa}{1+\kappa\delta_p}. \tag{D-7}$$

E. Entropic free energy

Here we present detailed intermediate steps that lead to the entropic free energy $F_{\rm ent}$ in Eq. 10, which is related to the number of ways (or multiplicity) W in which N_0 sites are occupied by (N_1+N_2) ions and N_p peptides. First, note that each peptide occupies Q sites. Here, we assume that peptides are distributed independently of each other, as in the Flory approach to a polymer solution[46].

If the "independent" binding of peptides is assumed, W can be readily obtained as

$$W=\left(\frac{\prod_{i=1}^{N_p}(N_0-(i-1)Q)}{N_p!}\right)\left(\frac{(N_0-QN_p)!}{N_1!N_2!(N_0-N_1-N_2-QN_p)!}\right). \tag{E-1}$$

The terms in the first parenthesis corresponds to the number of ways to distribute N_p peptides on the surface, assuming them to be indistinguishable and independent from each other. The remaining terms are just the usual formula for the multiplicity of (N_1+N_2) ions distributed on (N_0-QN_p) binding sites.

Taking the log of both sides, we find

$$\ln W=\ln\prod_{i=1}^{N_p}[N_0-(i-1)Q]-\ln(N_p!)+\ln\left[((N_0-QN_p)!\right]-\ln\left(N_1!\right)-\ln\left(N_2!\right)-\ln\left[(N_0-N_1-N_2-QN_p)!\right]. \tag{E-2}$$

Moreover, each term can be simplified by converting a sum into an integral, or equivalently, by using Stirling's formula $(\ln n!\approx n\ln n-n)$ for large n. The first two terms can be approximated by

$$[...]\approx\int_1^{N_p}\ln\left[N_0-(n-1)Q\right]dn-N_p\ln N_p+N_p\approx-\frac{(N_0-QN_p)}{Q}\ln\left(1-\frac{QN_p}{N_0}\right)-N_p\ln\frac{N_p}{N_0}. \tag{E-3}$$

The other terms are treated similarly:

$$\text{others}\approx(N_0-QN_p)\ln\left(1-\frac{QN_p}{N_0}\right)-N_1\ln\frac{N_1}{N_0}-N_2\ln\frac{N_2}{N_0}-(N_0-N_1-N_2-QN_p)\ln\left(1-\frac{N_1-N_2-QN_p}{N_0}\right). \tag{E-4}$$

All together, we can find the entropic term using $F_{\rm ent}=-\ln W$:

$$\begin{aligned}F_{\rm ent}\cdot N_0 &= N_1\ln\left(\frac{N_1}{N_0}\right)+N_2\ln\left(\frac{N_2}{N_0}\right)+N_p\ln\left(\frac{N_p}{N_0}\right)+(N_0-N_1-N_2-QN_p)\ln\left(1-\frac{N_1+N_2+QN_p}{N_0}\right)\\ &\quad+\left(\frac{1-Q}{Q}\right)(N_0-QN_p)\ln\left(1-\frac{QN_p}{N_0}\right).\end{aligned} \tag{E-5}$$

This is identical to the result in Eq. 10.

References

1 C. R. H. Raetz and C. Whitfield, Lipopolysaccharide Endotoxins, *Annu. Rev. Biochem.* **2002**, *71*, 635-700.

2 S. G. Wilkinson. Bacterial lipopolysaccharides – themes and variations. *Prog. Lipid Res.* **1996**, *35*, 283-343.

3 H. Nikaido, Molecular Basis of Bacterial Outer Membrane Permeability Revisited, *Microbiology and Molecular Biology Reviews*, **2003**, *67*, 593-656.

4 R. E. W. Hancock, Alterations in Outer Membrane Permeability, *Ann. Rev. Microbiol.* **1984**, *38*, 237-264.

5 L. Zhang, P. Dhillon, H. Yan, S. Farmer, and R. E. W. Hancock, Interactions of Bacterial Cationic Peptide Antibiotics with Outer and Cytoplasmic Membranes of Pseudomonas aeruginosa, *Antimicrob. Agents Chemother.* **2000**, *44*, 3317-3321.

6 K. Matsuzaki, K. Sugishita, and K. Miyajima, Interactions of an antimicrobial peptide, magainin 2, with lipopolysaccharide-containing liposomes as a model for outer membranes of Gram-negative bacteria, *FEBS Lett.* **1999**, *449*, 221-224.

7 N. A. Amro, et al., High-Resolution Atomic Force Microscopy Studies of the Escherichia coli Outer Membrane: Structural Basis for Permeability, *Langmuir* **2000**, *16*, 2789-2796.

8 M. Vaara, Agents that Increase the Permeability of the Outer Membrane, *Microbiol. Rev.* **1992**, 395-411.

9 L. Leive, Release of lipopolysaccharide by EDTA treatment of *E. coli*, *Biochem. Biophys. Res. Commun.* **1965**, *21*, 290-296.

10 L. Leive, A nonspecific increase in permeability in *Escherichia coli* produced by EDTA, *Proc. Nat. Acad. Sci. U.S.A.* **1965**, *53*, 745-750.

11 A. H. Delcour, Outer membrane permeability and antibiotic resistance, *Biochim. Biophys. Acta* **2009**, *1794*, 808-816.

12 M. Zasloff, Antimicrobial peptides of multicellular organisms, *Nature* **2002**, *415*, 389-395.

13 K. A. Brogden, Antimicrobial peptides: pore formers or metabolic inhibitor, *Nat. Rev. Microbiol.* **2005**, *3*, 238-250.

14 A. Peschel and H.-G. Sahl, The co-evolution of host cationic antimicrobial peptides and microbial resistance, *Nat. Rev. Microbiol.* **2006**, *4*, 529-536.

15 L. Guo et al., Lipid A Acylation and Bacterial Resistance against Vertebrate Antimicrobial Peptides. *Cell* **1998**, *95*, 189-198.

16 L. Ding et al., Interaction of Antimicrobial Peptides with Lipopolysaccharides, *Biochemistry* **2003**, *42*, 12251-12259.

17 E. A. Groisman, The Pleiotropic Two-Component Regulatory System PhoP-PhoQ, *J. Bacteriol.* **2001**, *183*, 1835-1842.

18 J. V. Hankins, J. A. Madsen, D. K. Giles, J. S. Brodbelt, and M. S. Trent, Amino acid addition to Vibrio cholerae LPS establishes a link between surface remodeling in Gram-positive and Gram-negative bacteria, *Proc. Natl. Acad. Sci. U. S. A.* **2012**, *109*, 8722-8727.

19 T. Abraham, S. R. Schooling, M. P. Nieh, N. Kucerka, T. J. Beveridge, and J. Katsaras, Neutron Diffraction Study of Pseudomonas aeruginosa Lipopolysaccharide Bilayers, *J. Phys. Chem. B* **2007**, *111*, 2477-2483.

20 N. Kučerka et al, Effect of Cations on the Structure of Bilayers Formed by Lipopolysaccharides Isolated from *Pseudomonas aeruginosa* PAO1, *J. Phys. Chem. B* **2008**, *112*, 8057-8062.

21 P. Garidela et al., Divalent cations affect chain mobility and aggregate structure of lipopolysaccharide from Salmonella minnesota reflected in a decrease of its biological activity, *Biochim. Biophys. Acta* **2005**, *1715*, 122-131.

22 S. Snyder, D. Kim, and T. J. McIntosh, Lipopolysaccharide Bilayer Structure: Effect of Chemotype, Core Mutations, Divalent Cations, and Temperature, *Biochemistry* **1999**, *38*, 10758-10767.

23 D. A. Pink et al., Divalent Calcium Ions Inhibit the Penetration of Protamine through the Polysaccharide Brush of the Outer Membrane of Gram-Negative Bacteria, *Langmuir* **2003**, *19*, 8852-8858.

24 E. Schneck et al., Quantitative determination of ion distributions in bacterial lipopolysaccharide membranes by grazing-incidence X-ray fluorescence, *Proc. Nat. Acad. Sci. U. S. A.* **2010**, *107*, 9147-51.

25 E. Schneck et al., Mechanical properties of interacting lipopolysaccharide membranes from bacteria mutants studied by specular and off-specular neutron scattering, *Phys. Rev. E* **2009**, *80*, 041929-1–041929-9.

26 K. Brandenburg, M. H. Koch, U. J. Seydel, Phase diagram of deep rough mutant lipopolysaccharide from Salmonella minnesota R595, *Struct. Biol.* **1992**, *108*, 93-106.

27 M. L. Henle, C. D. Santangelo, D. M. Patel, and P. A. Pincus, Distribution of counterions near discretely charged planes and rods, *Europhys. Lett.* **2004**, *66*, 284-290.

28 A. Travesset and D. Vaknin, Bjerrum pairing correlations at charged interfaces, *Europhys. Lett.* **2006**, *74*, 181-187.

29 H. O. Negrete, R. L. Rivers, A. H. Gough, M. Colombini, and M. L. Zeidel, Individual Leaflets of a Membrane Bilayer Can Independently Regulate Permeability, *J. Biol. Chem.* **1996**, *271*, 11627-11630.

30 H. W. Huang, Deformation free energy of bilayer membrane and its effect on gramicidin channel lifetime, *Biophys J.* **1986**, *50*,1061-1070.

31 J. Howe et al., Thermodynamic Analysis of the Lipopolysaccharide-Dependent Resistance of Gram-

Negative Bacteria against Polymyxin B, *Biophys. J.* **2007**, *92*, 2796-2805.

32 M.-T. Lee, W.-C. Hung, F.-Y. Chen and H. W. Huang, Mechanism and kinetics of pore formation in membranes by water-soluble amphipathic peptides, *Proc. Natl. Acad. Sci. U. S. A.* **2008**, *105*, 5087-5092.

33 S. Taheri-Araghi and B.-Y. Ha, Cationic antimicrobial peptides: a physical basis for their selective membrane-disrupting activity, *Soft Matter* **2010**, *6*, 1933-1940.

34 R. M. Epand and R. F. Epand, Chapter 7, Biophysical Analysis of Membrane-Targeting Antimicrobial Peptides: Membrane Properties and the Design of Peptides Specifically Targeting Gram-negative Bacteria in *Antimicrobial peptides discovery, design and novel therapeutic strategies* edited by G. Wang (Cabi, 2010).

35 S. Taheri-Araghi and B.-Y. Ha, Electrostatic Bending of Lipid Membranes: How Are Lipid and Electrostatic Properties Interrelated? *Langmuir* **2010**, *26*, 14737-14746.

36 See for instance *Molecular Driving Forces: Statistical Thermodynamics in Biology, Chemistry, Physics, and Nanoscience*, 2nd Edt., K. A. Dill and S. Bromberg (Garland Science, 2010).

37 T. L. Hill, *An Introduction to Statistical Thermodynamics* (Dover Publications, 1986).

38 See M. E. Fisher and Y. Levin, *Phys. Rev. Lett.* **1993**, *71*, 3826-3829 and references therein.

39 See for instance *Statistical Mechanics*, D. A. McQuarrie (University Science Books, 2000).

40 J. N. Israelachvili, *Intermolecular and Surface Forces*, 3rd Edt. (Academic Press, 2011).

41 S. Taheri-Araghi and B.-Y. Ha, Charge renormalization and inversion of a highly charged lipid bilayer: Effects of dielectric discontinuities and charge correlations, *Phys. Rev. E.* **2005**, *72*, 021508-1–021508-10.

42 P. C. H. Mitchell, Metal Complexes of EDTA: An Exercise in Data Interpretation, *J. Chem. Educ.* **1997**, *74*, 1235-1237.

43 K. Matsuzaki, Control of cell selectivity of antimicrobial peptides, *Biochim. Biophys. Acta* **2009**, *1788*, 1687-1692.

44 M. N. Melo, R. Ferre, and M. A. R. B. Castanho, Antimicrobial peptides: linking partition, activity and high membrane-bound concentrations, *Nat. Rev. Microbiol.* **2009**, *7*, 245-250.

45 For an earlier attempt to derive the electrostatic energy of the LPS layer, excluding F_{LC}, see R. R. Farzami, *Electrostatic Interactions of Peptides with Lipid Membranes: Competitive Binding between Cationic Peptides and Divalent Counterions* (MSc thesis, University of Waterloo, 2010).

46 P.-G. Gennes, *Scaling Concepts in Polymer Physics* (Cornell University Press, 1979).